Design of an Energy Management System Using a Distribution Class Locational Marginal Price as a Discrete Control Signal

by

Jesse Boyd

A Thesis Presented in Partial Fulfillment
of the Requirements for the Degree
Master of Science

Approved July 2013 by the
Graduate Supervisory Committee:

Gerald Heydt, Chair
Rajib Datta
Lalitha Sankar

ARIZONA STATE UNIVERSITY

August 2013

ABSTRACT

The subject of this thesis is distribution level load management using a pricing signal in a Smart Grid infrastructure. The Smart Grid implements advanced meters, sensory devices and near real time communication between the elements of the system, including the distribution operator and the customer. A stated objective of the Smart Grid is to use sensory information to operate the electrical power grid more efficiently and cost effectively. One potential function of the Smart Grid is energy management at the distribution level, namely at the individual customer. The Smart Grid allows control of distribution level devices, including distributed energy storage and distributed generation, in operational real time. One method of load control uses an electric energy price as a control signal. The control is achieved through customer preference as the customer allows loads to respond to a dynamic pricing signal.

In this thesis, a pricing signal is used to control loads for energy management at the distribution level. The model for the energy management system is created and analyzed in the z-domain due to the envisioned discrete time implementation. Test cases are used to illustrate stability and performance by analytic calculations using Mathcad and by simulation using Matlab Simulink. The envisioned control strategy is applied to the Future Renewable Electric Energy Distribution Management (FREEDM) system. The FREEDM system implements electronic (semiconductor) controls and therefore makes the proposed energy management feasible.

The pricing control strategy is demonstrated to be an effective method of performing energy management in a distribution system. It is also shown that stability and near

optimal response can be achieved by controlling the parameters of the system. Additionally, the communication bandwidth requirements for a pricing control signal are evaluated.

I dedicate this thesis to my parents, Matthew and Helen Boyd, who taught me to value education, excellence, and beneficence. These values enabled me to accomplish this thesis and I hope to continue to uphold and impart them. I also dedicate this thesis to my sister, Casey, whose aspirations continue to inspire me. She has been a great encouragement and resource throughout this process. Finally, I dedicate this work to my friends who have all shown their support, excitement, and belief in this work. All of their support made this thesis possible.

ACKNOWLEDGEMENTS

I would like to give thanks first to my advisor and chair Dr. Gerald T. Heydt for the opportunity to work with him and for his guidance, correction, and encouragement through this master's degree. I also thank Dr. Rajib Datta and Dr. Lalitha Sankar for their time and effort in being a part of my supervisory committee.

Funding for this research was provided by the National Science Foundation under the Engineering Research Center program, grant EEC-08212121. The author acknowledges the Future Renewable Electric Energy Distribution and Management Center (FREEDM) for its support.

Finally, I want to thank Arizona State University for providing the opportunity and the institution for me to pursue my goal of advanced education.

TABLE OF CONTENTS

Page

CHAPTER Page

Page

LIST OF TABLES

Table Page

LIST OF FIGURES

Figure Page

Figure Page

Figure Page

NOMENCLATURE

a	Scalar coefficient (unitless)
b	Scalar coefficient (kW)
B	Feedback gain
B*	‘Optimal’ value of feedback gain B
B^k	Feedback gain vector for pricing node k
B_{max}	Maximum battery capacity (kWh)
B_{min}	Minimum battery capacity (kWh)
BW	Bandwidth (Hz, kHz)
C	Channel capacity (bits per second)
c	Scalar coefficient (kW^2)
$c_1(x)$	Cost function of x
$c_2(x)$	Cost function of x
DES	Distributed energy storage
DESD	Distributed energy storage device
DG	Distributed generation
DLMP	Distribution locational marginal price
e	Euler’s number
E(·)	Expectation function

E_C	Cross-price elasticity of electric energy demand
E_S	Self-price elasticity of electric energy demand
EMS	Energy management system
f	Power flow into a battery
FREEDM	Future Renewable Electric Energy Distribution Management
g_n	Power flow oriented from an energy storage device into the grid
H	Transfer function
i	Index variable
I	Identity matrix
I(x)	Aggregate objective function
ISE	Integral square error
ISE_z	Integral square error as defined in the z-domain
j	Distribution node index variable, $\sqrt{-1}$
k	Distribution node index variable
l	Distribution line
ℓ_g	Active power loss due to generation
ℓ_n	Active power loss due to energy storage and generation at sample n
ℓ_s	Active power loss due to energy storage
L	Load control signal

L_0	Nominal load level
L_{new}	Real time updated load level
LMP	Transmission locational marginal price
m	Sample number
MOP	Multi-objective programming
N	Number of samples, number of busses
n	Sample number
p	Price for a good, probability
P	Square, positive semi-definite matrix
p_i	Probability of the i^{th} scenario
P_k	Power demand
P_l	Power flow in line l
P_{loss}	Real power loss
q	Demand of a good, vector
r	Scalar
s	Laplace domain variable, power flow into of the energy storage device
s_n	Power flow oriented from the grid into an energy storage device
SNR	Signal-to-noise ratio
t	Time

T	Sample time period
u	Binary variable representing positive (1) or zero (0) power flow out of the battery
v	Binary variable representing positive (1) or zero (0) power flow into the battery
w_1	Scalar weight for $c_1(x)$ in a multi-objective optimization problem
w_2	Scalar weight for $c_1(x)$ in a multi-objective optimization problem
w_3	Scalar weight for $c_1(x)$ in a multi-objective optimization problem
z	z-transform complex variable
X	z-domain control system input
Y	z-domain control system output
Z	Transformation from the time domain to the z-domain
α	Loss multiplier for the square of the generation power level (kW^{-1})
β	Loss multiplier to the generation power level (kW/kW)
γ	Loss constant for generation power level (kW)
δ_0	Distribution locational marginal price forecast
δ	Distribution locational marginal price
∂	Derivative operator
ΔL	Deviation of load control signal from nominal load
Δp	Change in price of a good

Δq	Change in demand of a good
$\Delta\delta$	Difference between real time DLMP and forecast DLMP
ε	Price elasticity of demand
$\varepsilon_{m,n}$	Price elasticity of demand for price change at sample m and demand response at sample n
η	Error
λ_n	Electric energy forecasted price ($/kWh) at the time of sample n
μ_{cap}	Shadow price for battery capacity constraint
μ_{ch}	Shadow price for balance of charge constraint
π	Participation factor
τ	Time
ϕ	Mapped variable, angle
χ	Loss multiplier for the square of the charging power level (kW^{-1})
ψ	Loss multiplier to the storage power level (kW/kW)
ω	Loss constant for storage power level (kW)
$\preceq$	Element-wise less-than or equal-to
$\forall$	For all

CHAPTER 1

DEMAND RESPONSE IN THE SMART GRID

1.1 Scope and objectives of this research

This research relates to electric power distribution engineering. The main objective of this thesis is to examine the use of a pricing signal as an energy management control signal. The scope of the study is relegated to primary power distribution systems (e.g., 15 kV class) in which some control is possible for load level energy management. The goal is a more effective utilization of the electric power distribution system. A further scope and objective is to model an implementation of the 'Smart Grid' as promoted by the Department of Energy in the United States [1]. The framework of the distribution system is assumed to be that promoted by the Future Renewable Electric Energy Distribution Management (FREEDM) center [2].

1.2 Load management through pricing signal control

The implementation of a pricing signal for distribution level load control in a practical system requires a novel distribution infrastructure. Such an infrastructure is envisioned in the *Smart Grid*. The Energy Independence and Security Act of 2007 describes the Smart Grid with the following characteristics [3]:

1. Increased digital information and control
2. Dynamic grid operations
3. Integration of distributed resources
4. Development of demand reduction methods
5. Deployment of automated, real time, interactive technologies

6. Integration of appliances with communication and automated control capabilities
7. Increased energy storage technologies and integration
8. Timely communication between utilities and consumers

Demand response is a prospective Smart Grid application which can potentially reduce power demand using a pricing mechanism. The economic idea behind demand response is that demand for electric energy generally changes inversely with the price of electric energy. Demand response programs are typically used to reduce energy consumption either during peak loading periods or at some other critical time. The subject of demand response, or more generally 'energy management,' is discussed extensively in the literature, e.g., [4-9].

A main concept behind demand response is a shift away from the use of a single fixed price for electric energy. The problem with setting a non-varying energy price is that it may or may not reflect the costs of providing that energy. Figure 1.1 shows a pictorial of this problem. The demand for power under a fixed price (D_1) can be higher than it would be under a variable price which is set according to the market costs. Since market costs rise with rising demand, during the time of peak use, customers may end up paying below the cost to provide that electric energy. Raising the price of electric energy in real time can alleviate this problem, allowing the price to reflect rising costs and causing the demand to decrease in response (D_2). Market efficiency is increased when the price is allowed to track the costs of providing electric energy [10].

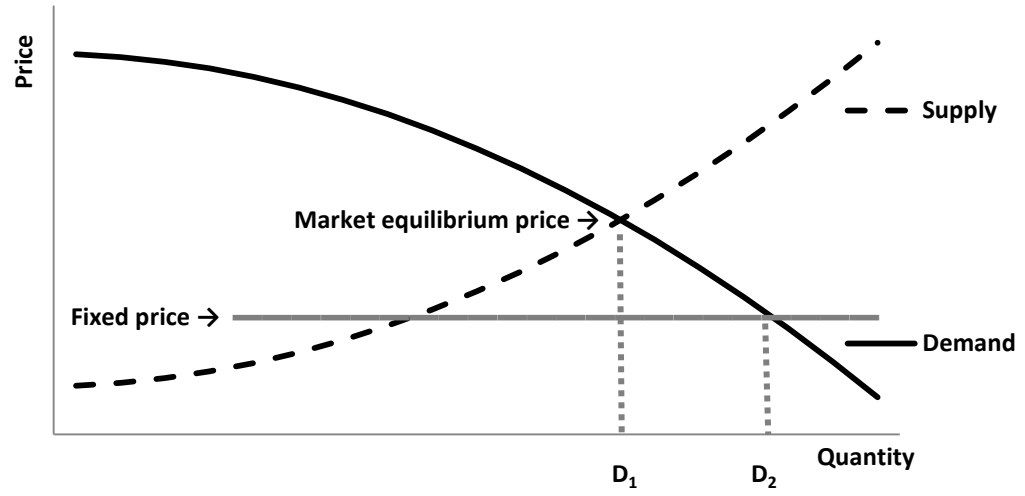

Figure 1.1 Demonstration of a potential scenario for a fixed price vs. a market clearing price.

Since the level of the demand can, to an extent, be altered by the price, the price of electric energy may be viewed as a control signal. This thesis develops an energy management system based around a pricing control signal as in the block diagram of Figure 1.2. In this diagram, there is interdependency between the price of electric energy and consumption, as indicated by the feedback signal through the sensory measurements block. This feedback relationship is also intuitive: demand changes affect the system costs; system costs, in turn, affect the price of electric energy. This model can be considered a *closed-loop control system* and is analyzed using linear time-invariant discrete control theory. For this thesis, the pricing signal in the Smart Grid is envisioned as updating in discrete time increments. In actual implementation, the length of update time increments may vary and be limited by measurement times, calculation times and communication delays. However, for this evaluation the time increments are considered fixed.

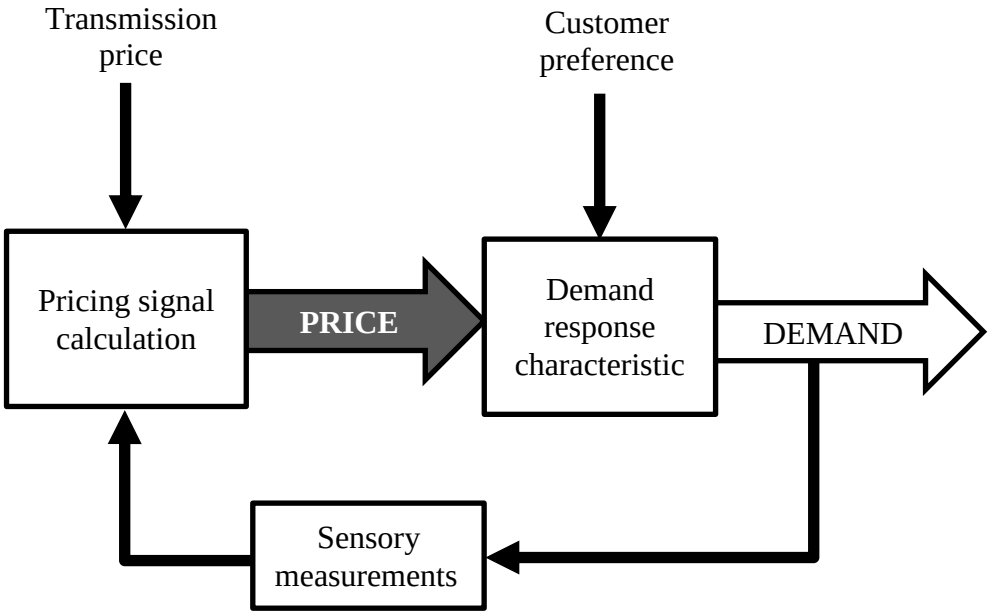

Figure 1.2 Block diagram demonstrating the basic concept of demand response using a price control signal.

The effectiveness of this pricing control strategy depends on customer response to price incentives. This suggests the concept of *price elasticity*. Price elasticity is an economic measurement of demand change in response to a price change. This concept is discussed in a subsequent section devoted entirely to price elasticity. Collecting the aforementioned elements, this research models the price controlled energy management system as a closed-loop control system in the discrete time domain using elasticity to approximate customer response. The big picture of the pricing control strategy, including inputs, technological infrastructure and potential benefits is shown in Figure 1.3.

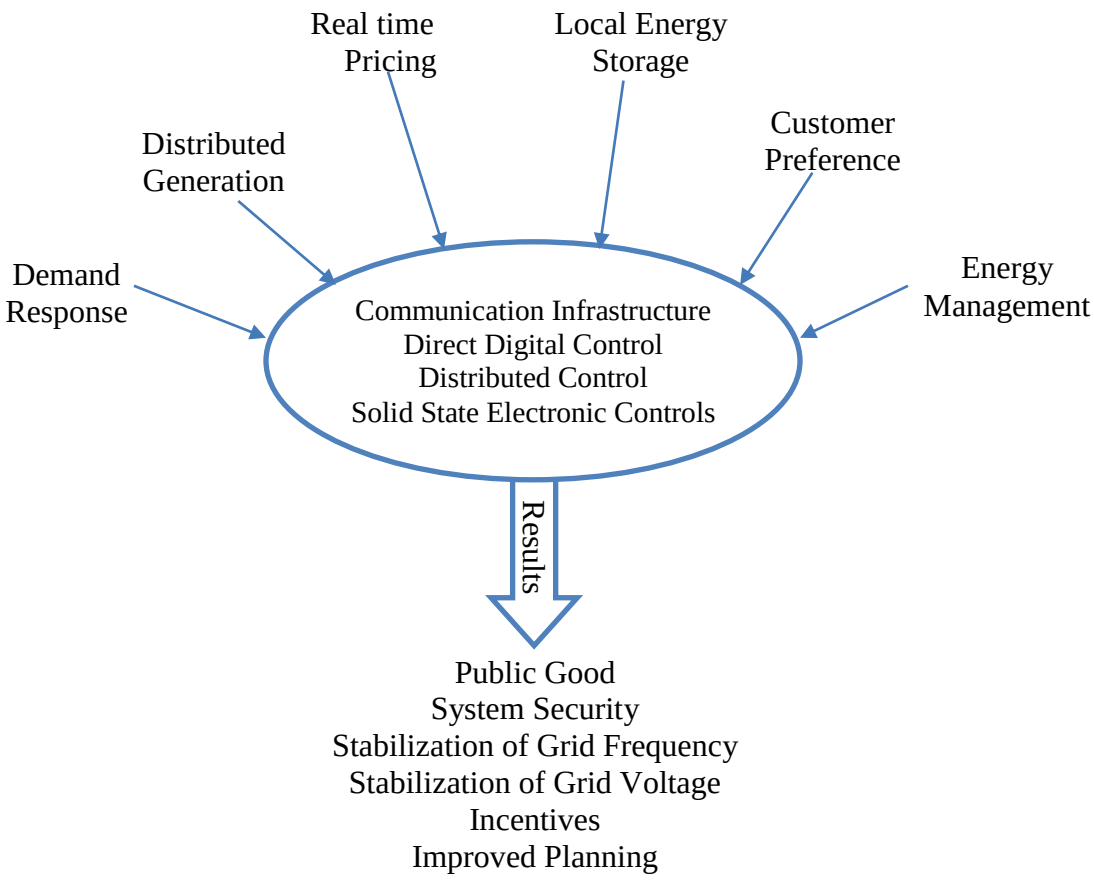

Figure 1.3 The use of a control strategy for demand response can result in security benefits, cost savings and social welfare.

1.3 Introduction to the FREEDM project

The Future Renewable Electric Energy Distribution Management (FREEDM) Systems Center was founded by the National Science Foundation in 2009 to promote innovative technologies in power distribution. The universities participating in the FREEDM systems center include North Carolina State University, Raleigh and Arizona State University, Tempe. The goal of the FREEDM research is to develop knowledge in energy storage, power semiconductor technologies and enabling technologies for system demonstration [11]. The envisioned FREEDM system is an electric power distribution system which includes distributed grid intelligence, internet connection between subnetworks,

solid state transformers, fault isolation devices, distributed energy storage and distributed renewable energy generation [2]. Some of the envisioned capabilities of the FREEDM system are islanding operation, intelligent control of distributed resources and plug-and-play ability for connecting devices to the grid [12]. This thesis contributes to the FREEDM systems research by examining the control of loads and energy storage devices using a pricing signal. A preliminary work done on stability analysis of a price controlled energy management system is [13].

1.4 Demand response literature overview

As early as the 1930s, it was argued that electric energy should be priced with some consideration to demand response [14]. Demand response today is envisioned as a method to reduce the costs of electric energy by discouraging customers from using electric energy from the grid during high demand periods. These high demand periods carry disproportionate costs for the power grid largely due to the requisite generation and transmission capacity needed to meet this demand [15]. The highest 100 hours of the year are estimated to contribute to between ten and twenty percent of electricity costs [16]. Demand-side energy management can help defray these costs. Perhaps the most well-known demand-side energy management technique is *peak shaving*. The objective of peak shaving is to reduce the peak power demand by controlling deferrable loads in the system [17]. Peak shaving has been demonstrated to reduce system costs by as much as twenty five percent [18]. Utilities have reduced peak period costs by implementing demand response programs, including real time pricing, time-of-use pricing, and critical peak-pricing programs [19]. Full customer participation in such demand response programs is projected to reduce peak demand by as much as 30% [20]. The reduction in peak

electric power demand is a result of load management and reduction, distributed generation, distributed energy storage, development and implementation of more efficient technologies and public awareness.

Advances in information technology are expanding the potential usefulness of demand response [21] by creating the opportunity to turn the power grid into a Smart Grid [22]. As the communication of prices approaches real time, loads will be able to more precisely optimize energy use, generation, and storage [23-24] according to customer preference [25-26]. A method developed in [27] for aggregating demand response data could be used to more accurately predict customer response to operational real time changes in price. Using a near real time pricing signal, the utility could potentially control the load profile [28], increase system security [29], stabilize grid frequency [30] and more [31-32]. This level of control will require an advanced communication infrastructure [33] and will likely impact utility planning [34], grid operations [35] and energy markets [36-38]. An alternative to a price-driven demand response program is direct control of loads through a demand dispatch control signal [39]. However, even a direct control over loads can use price as a control signal. Since the amount of electric energy demand is dependent on price, the calculation of the pricing signal is central to the operation of a demand response driven Smart Grid. One potential pricing control signal has been denominated as the distribution locational marginal price (DLMP) and its calculation is discussed further in the next section.

1.5 Distribution locational marginal price literature review

Early in the life of the power grid, it was argued that the prevailing flat rate of electric energy was inferior to a more specific price which could vary with the type of

load, location of the load, and time of energy consumption [40]. A more precise price is based on a transmission level locational marginal price (LMP) [41] calculation. However, a LMP would not suffice for the precise control of loads anticipated in the Smart Grid. As the mathematical formulation evolved, a method for deriving a *spot price* for electric energy at the distribution level was developed [42]. The spot price was preferred because it reflected cost of energy more accurately by discerning between time and location of the electric energy demand on the distribution level [43]. The Smart Grid infrastructure will allow the communication and precise system state calculations which are required for a real time spot price. This in itself may accomplish some goals of the Smart Grid, including reducing costs, peak demand and CO_2 emissions [44]. The envisioned price as a control signal is not merely a more accurate representation of costs, however, but also a means of control for other desired ends. These ends may include increased distributed generation, use of distributed energy storage and increased efficiency. Therefore, a modified LMP has been formulated at the distribution level for use in Smart Grid applications and denominated the distribution locational marginal price (DLMP). This may be formulated in multiple ways to achieve desired ends. One formula for the DLMP is [45]

$$\delta_k = w_1 \sum_{i=1}^{N} \pi_i LMP_i + w_2 \sum_{l=1}^{M} \frac{\partial P_{loss,l}}{\partial P_k} + w_3 \sum_{l=1}^{M} \frac{\partial P_l}{\partial P_k} \tag{1.1}$$

In (1.1), δ_k is the DLMP at distribution node *k*, the *w* coefficients are weights given to the different components of the formula, *N* is the number of busses, *M* is the number of lines and π_i is the generation participation factor. This formulation takes into account three factors in order to price energy consumption: 1) the cost of the LMP from the transmission system; 2) the line power losses; and 3) the congestion constraints. Each of these ele-

ments is calculated relative to the impact of the load at node *k*. Note that this DLMP is not precisely the marginal cost of energy at node *k*, but is an approximation of the marginal cost. Other formulations for the DLMP are given in [45]. Still more electric energy price formulations include pricing for reliability [46], loss reduction including game theory [47], and demand response forecasting [48]. The precise DLMP calculation is not the focus of this thesis. Rather, this thesis concerns the DLMP as a signal in a control system. The formula used in this thesis to update the DLMP is a general formula

$$\delta_k = \delta_{0,k} + \sum_j B_{k,j}\,\Delta L_j + d \tag{1.2}$$

where $\delta_{0,k}$ is the nominal DLMP calculated value at node *k*, δ_k is the updated value, B is the feedback gain and *d* is a small-signal control. The changes in demand at any node may impact every other node, so ΔL is indexed for each node in the distribution system, *j*. The coefficient *B* is in \$/(kW^{2}h) and represents a linear approximation to the change in the DLMP at node *k* for a change in load at each The assumption of (1.2) is that the DLMP dependence on load levels can be approximated as linear for small perturbations around the nominal DLMP.

1.6 Price elasticity

The *price elasticity of demand* is an economic formula of the change in the demanded quantity of a product in response to a change in its price. It can be viewed as the normalized inverse of the slope of the demand curve. The price elasticity of demand is generally assumed to be negative, but is not necessarily uniform since the slope depends on the operating point on the demand curve. The graph in Figure 1.4 demonstrates this concept. The definition of price elasticity of demand is elaborated in [49] as,

$$\varepsilon = \frac{\frac{\Delta q}{q_0}}{\frac{\Delta p}{p_0}} \tag{1.3}$$

where Δq is the change in power demand, Δp is the change in price of electric energy, and q_0 and p_0 define the operating point on the demand curve. If the price of electric energy rises, the concept of elasticity predicts that the consumption should fall assuming that the loads have some negative price elasticity. This is apparent from a rearrangement of (1.3),

$$\frac{\Delta q}{q_0} = \varepsilon \frac{\Delta p}{p_0}. \tag{1.4}$$

However, not all loads would respond to small or even large changes in price. It becomes important, then, to investigate what loads are curtailable, what level of total demand is controlled and what the side-effects of curtailing a load are. In other words, it is necessary to find the price elasticities of the loads in the system.

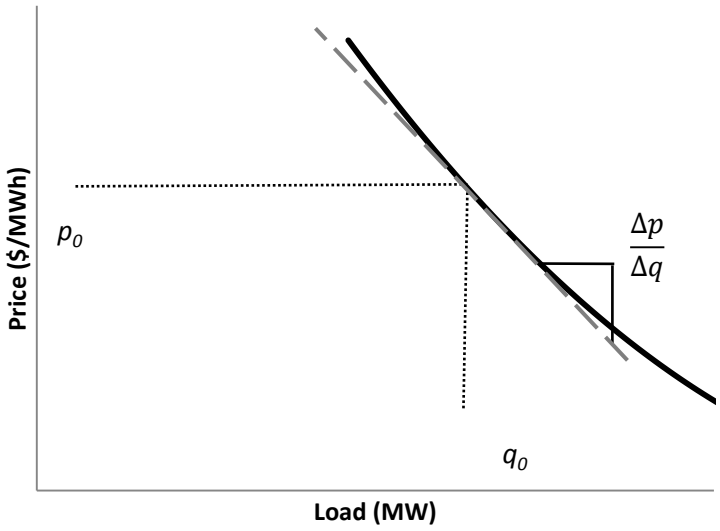

Figure 1.4 The demand curve has a slope ($\Delta p/\Delta q$) at a particular price and quantity (p_0 and q_0).

One of the consequences of curtailing a load is that it may impact subsequent energy use. For example, if an air conditioning unit is turned off in response to a high price, eventually that air conditioner is likely to be turned back on and must consequently run longer to cool off a warmer room. This brings up another economic concept which splits the general term of price elasticity into the more specific terms of *self-* and *cross*-price elasticity. Self-price elasticity (also known as own-price elasticity) is the change of the demand of a good cause by the change in price of that good. In the case of electric energy, it is the response of electric energy demand to a simultaneous change in price. Self-price elasticity is generally negative, since an increased price at time t would tend to cause a decrease in demand at time t. The second division of elasticity is cross-price elasticity. This has to do with the change in consumption of either a *substitute* product or a *complementary* product in response to a change in price. In other words, it is the change in demand of product B due to the change in price of product A. In this thesis, the products are all electric energy and the cross products are electric energy at a different time. In other words, an electric energy price change at time t results in electric energy consumption change at time $t + \tau$. The idea is that the energy consumption may either be delayed due to a higher price or that the higher price could make an associated electric energy consumption change. Therefore, cross-price elasticity can be either positive (substitute) or negative (complement). One reason it might be negative is if some extended process did not begin because of an increase in energy price. Since the process did not begin at time t, it may no longer require energy at time $t + \tau$. Alternately, cross-price elasticity can be positive if the energy demand is somehow delayed by an increase in price. If an appliance did not run at time t, it is more likely to run at $t + \tau$. This is demonstrated picto-

rially in Figure 1.5. In these graphs, E_S is the self-price elasticity of demand and E_C is the cross-price elasticity of demand. The load change L_{new} is a deviation from the nominal load L_0 in reaction to a price increase enduring from time t_1 to t_2.

Self- and cross-price elasticity values can be useful in predicting demand response to a pricing signal. This may be represented in a matrix of elasticity values representing the changes in load at each particular time relative to the changes in price at each time. Using N as the limit of the extent of time under consideration, this could look like [49],

$$\frac{\Delta q_m}{q_0} = \sum_{n=1}^{N} \varepsilon_{m,n} \frac{\Delta p_n}{p_0} \tag{1.5}$$

where m and n index time periods which both add up to N periods and $N-1$ is the total number of periods considered for cross-elasticity. The equation (1.5) includes both self-elasticity and cross-elasticity. The self-elasticity for each time is the diagonal of the matrix, where the elements represent a change in demand simultaneous with the change in price (i.e., $m = n$). Therefore, the diagonals of ε are generally negative. The cross-price elasticity for each time is the non-diagonal row elements for the row corresponding to each time m. These values determine how the demand at time m changes according to a change in price at other times ($m \neq n$). For instance, if price in the afternoon is higher than expected, it might cause consumption to shift slightly to the evening. Therefore, cross-price elasticity values are often positive. An increase in price at one time tends to decrease use at that time and increase use at other times. If a consumer must have the same amount of total energy, the self-price and cross-price elasticity values sum exactly to zero (assuming that the operating point remains constant)

$$\sum_{n=1}^{N} \varepsilon_{m,n} = 0. \tag{1.6}$$

Electric energy is generally considered to be an *inelastic* good. This is because the amount of power demanded is not largely dependent on the price. In economic theory, the threshold for an 'elastic' good is unitary elasticity. That is, for every percent change in price there is a percent change in consumption. Electric energy is well below this threshold. Typical self-price elasticity values range from 0 to -0.50 [50] and typical values for cross-price elasticity in demand response programs range from 0 to 0.30 [51]. Note that these are *short term* elasticities in response to time-of-use prices. The length of time between the knowledge of the price and the time of energy use is typically one day. Long term elasticity has a greater time period in mind and has been examined by a number of other studies, e.g.; [52-54]. In this thesis, short term elasticity is used to estimate demand response to an operational real time price mechanism. The low magnitudes for real time price elasticity could suggest that the price of energy may not significantly change energy consumption, as argued in [50]. However, the envisioned system of the future has a high level of control and communication that could make electric energy more price-elastic. One significant addition to the future grid is the demand response of energy storage devices. These can have price elasticities well above unitary. Another difference is the level of intelligent control over appliances. Therefore, the demand response to a price mechanism may be significantly larger than the estimates found in the above studies.

A couple of comments are pertinent concerning the use of elasticity to estimate responsive loads. First, the elasticity matrix is a way to perform small, linear changes around an operating point (p_0, q_0). However, it does not perform the non-linear algorithm needed to set the operating point. This must be done by some other method. Second, using elasticity to model responsive loads assumes that the demand change can be approx-

imated by a linear relationship to price change, which may not be true for large changes in price or loads that have discrete levels of power consumption. The use of elasticity values provides a way to linearly approximate a change in demand to a change in price, but does not determine *initial* demand at that price and does not model *non-linear* changes in demand.

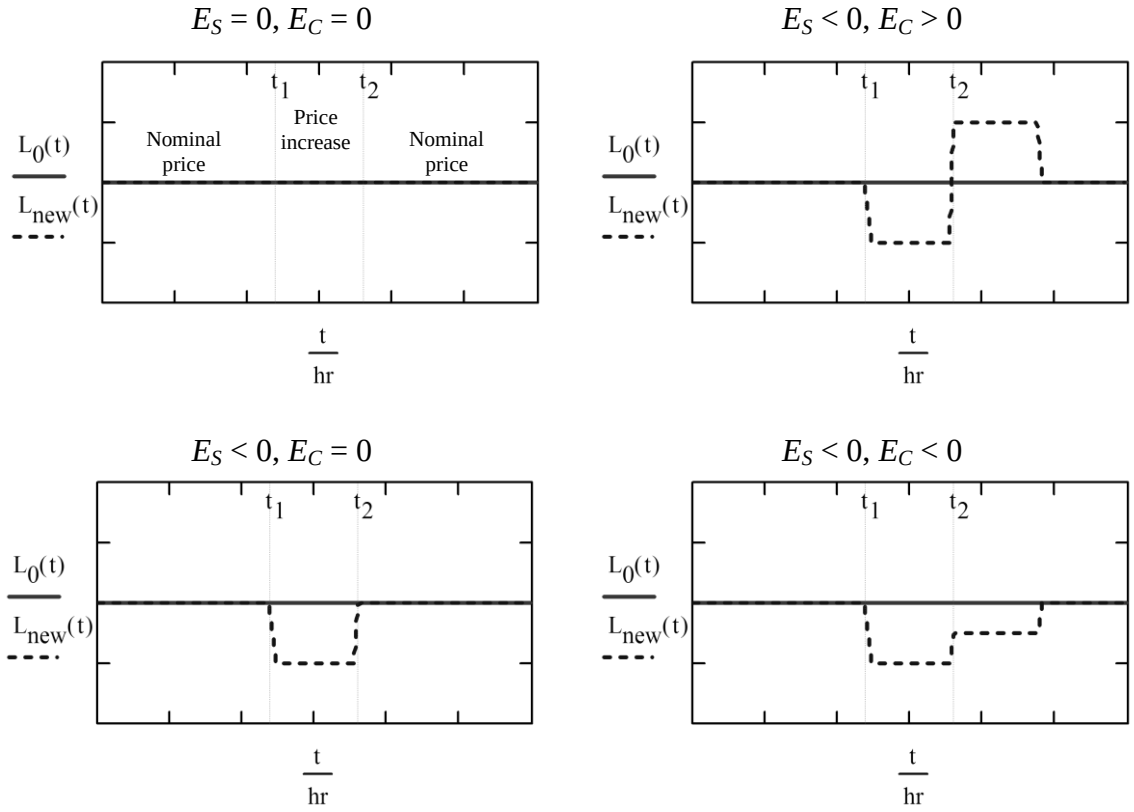

Figure 1.5 Pictorial demonstrations of different price elasticity scenarios.

1.7 The *z*-transform for discrete systems

Delay between updates in the pricing signal is assumed in the implementation of a price controlled energy management system. Treating this delay as sample periods allows

the system to be modeled as a discrete control system which can be analyzed in the *z*-domain. The one-sided *z*-transform is defined by

$$Z\{f(nT)\} = F(z) = \sum_{n=0}^{\infty} f(nT)z^{-n} \tag{1.7}$$

where *f(t)* is a function defined for $t \geq 0$, the sampling time *T* is positive, and the sample number is indicated by *n*. Some common *z*-domain operations and functions are given in Table 1.1.

Table 1.1 Some common functions and their *z*-domain transforms.

Description	Time domain representation	*z*-domain transformation
General function	$f(nT)$	$F(z) = \sum_{n=0}^{\infty} f(nT)z^{-n}$
Time delay	$f(nT - kT)$	$z^{-k}F(z)$
Integration	$\sum_{k=-\infty}^{n} f(kT)$	$\frac{z}{z-1}F(z)$
Unit step	$u(nT)$	$\frac{1}{1-z^{-1}}$
Impulse	$\delta(nT)$	1

1.8 Organization of this thesis

Chapter 1 has introduced some fundamental concepts which serve as a foundation for the work in this thesis, including demand response, DLMP, price elasticity and the *z*-transform. The more advanced theoretical concepts of self-price and cross-price elasticity, z-domain analysis, and integral square error as a performance index for a discrete time

control system are kept for Chapter 2. Also in Chapter 2, a linear shift-invariant model of the price controlled energy management system is created in the *z*-domain. Chapter 3 is dedicated to developing a distributed energy storage power flow optimization program in order to include energy storage as a load in the EMS model. Some test cases are presented for illustration of the control strategy in Chapter 4 including a single load case, a multiple load case, a case with energy storage and a case with uncertain load. Chapter 5 makes some conclusions about the study and recommendations for future work. The Appendix contains the pertinent Matlab code, Mathcad symbolic and numerical analysis and Simulink models along with relevant plots.

CHAPTER 2

ELASTICITY, STABILITY AND COMMUNICATION IN A PRICE CONTROLLED SYSTEM

2.1 Model of a pricing signal controlled system

The main idea behind the price controlled system is that a near real time pricing signal can be used to accomplish some of the goals of the Smart Grid. These goals include customer response to a transmitted dynamic price, control of energy storage to reduce peak demand, incentives for distributed energy resources and a dynamic price response to the system state. Using the concepts of elasticity and DLMP pricing signal discussed in Chapter 1, Figure 2.1 was created as a conceptual model for the envisioned control system. In this diagram, the DLMP calculation is dependent on three inputs: the forecasted DLMP, the feedback from the load through a gain block B and a small-signal control d. The load control algorithm block is not defined for this thesis however it is assumed to manage the load in two ways. First, it determines the *nominal* level for the loads using a forecast of the DLMP values. For instance, if the load is a battery, the algorithm may control the battery to store energy during low predicted DLMP and release energy during high predicted DLMP. The second way the load control algorithm block manages the load is by producing the price elasticity of demand matrix, E. Since the load control algorithm uses a predicted price and not the real time price, the load value must be updated to the real time pricing signal. The conceptual model in Figure 2.1 is used to derive the z-domain model in Section 2.3.

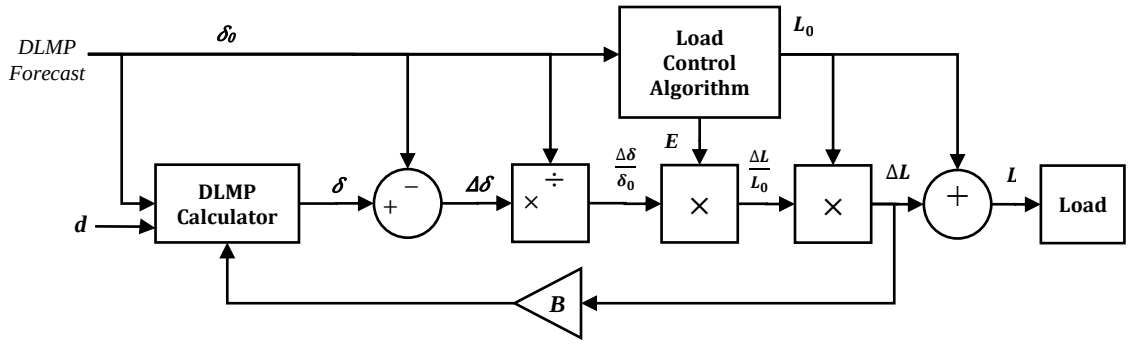

Figure 2.1 Block diagram of a pricing signal controlled energy management system

2.2 Price elasticity for electric energy demand in the *z*-domain

In order to model the behavior of customers to changing energy prices, the concept of price elasticity of energy demand is used. The formula may be written as

$$\varepsilon_{m,n} = \frac{\Delta L_m}{\Delta \delta_n} \frac{\delta_{0,n}}{L_{0,m}} \tag{2.1}$$

where ΔL_m is the change in the load at time sample m and $\Delta \delta_n$ is the change in distribution locational marginal price of electric energy at time sample n. The time is incremented in discrete intervals representing the delay between pricing signal updates caused by delays in the system. This is represented in the z-domain by the multiplier z^{-1}. This can be used to calculate the change in demand at time m in response to the change in price at time n by reworking 1.4 in the z-domain. An important distinction is needed here: the energy demand can only change in response to past real time price changes since the future real time price is not yet known. Reworking (1.4) in the z-domain yields:

$$\Delta L(z) = L_0 E_s \frac{\Delta \delta(z)}{\delta_0} + L_0 \sum_{n=1}^{N} E_{Cn} \frac{\Delta \delta(z)}{\delta_0} z^{-n}. \tag{2.2}$$

The z^{-n} multiplier represents a delay by n samples. In this way the cross-price elasticity values are used to adjust *future* load levels. The integer N is the total number of delays

considered for cross-elasticity, L_0 is the nominal load level, as calculated by the load control algorithm. It is important to note that the values L_0, E_S, E_{Cn}, and δ_0 may change in an actual system as the time increments, but they are treated as constants in this formula.

2.3 Linear *z*-domain model of a price controlled EMS

A causal linear system is bounded input bounded output (BIBO) stable if for any bounded input, the output is also bounded. In the *z*-domain, this is indicated when the poles of the transfer function all lie inside the unit circle. For the analysis in this thesis, the price controlled energy management system (EMS) is represented as a linear system in the *z*-domain. This allows the assessment of the system using BIBO stability analysis. The model of Figure 2.2 shows the resulting linear system.

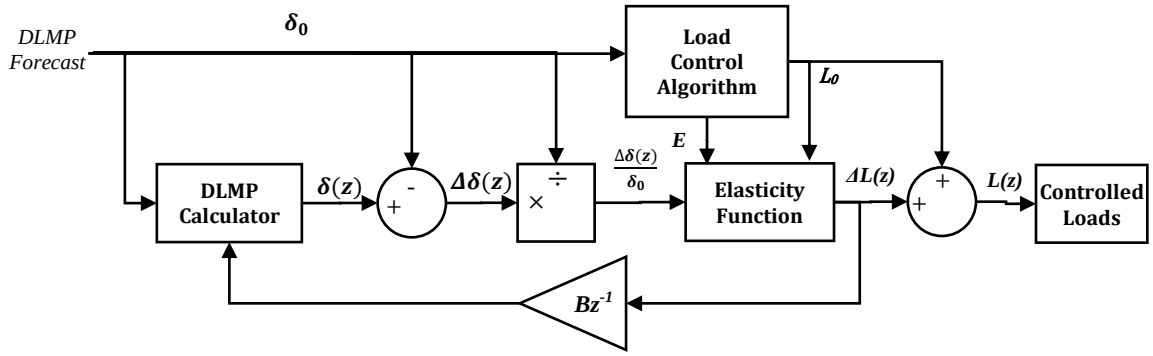

Figure 2.2 Block diagram of the linear *z*-domain price controlled EMS.

2.4 Stability and ISE in a discrete time system

For linear discrete systems, stability in the *z*-domain can be assessed by the location of the poles of the transfer function. Bounded input, bounded output (BIBO) stability is ensured when the impulse response of the system (i.e., the transfer function) has poles within the unit circle. For a single input single output linear discrete system, BIBO stability can be evaluated by

$$H(z) = Z\{h(t)\} = \frac{Y(z)}{X(z)} \tag{2.3}$$

where *H(z)* is the transfer function of the system, *Y* is the output of the system and *X* is the system input in the *z*-domain. Note that *H(z)* is a *z*-transform of the impulse response of the system, namely *h(nT)* where *n* is the running sample number and *T* is the sample time. BIBO stability of a system in the *z*-domain system is determined by the location of the poles of the transfer function. This observation may be viewed as an analog to the continuous case in which the one sided Laplace transform is used to find system stability for a continuous system with transfer function *H(s).* For the continuous case, poles in the right half plane result in exponentially increasing time domain response, and therefore right half plane poles of *H(s)* are disallowed for BIBO stability. Axis poles are also disallowed because a bounded input may result in a duplicate pole on the $j\omega$ axis thus causing an unbounded output. The same phenomena occur in discrete systems. Mapping the left-hand side poles in the *s*-domain into the *z*-domain shows that BIBO stability in the *z*-domain is ensured by poles inside the unit circle.

In the case of multiple-input multiple-output (MIMO) control systems, the BIBO stability of the system can be determined by the transfer matrix, whose elements are defined as

$$H_{j,k}(z) = \frac{Y_j(z)}{X_k(z)} \tag{2.4}$$

where Y_j is the j^{th} output and X_k is the k^{th} input variable. If each of these transfer function elements within the transfer function matrix is BIBO stable then the whole system is considered BIBO stable.

The end objective in the application addressed here is energy management using a pricing signal. Obviously BIBO stability is required. The stability of the control system in this application is not to be confused with 'stability' of electric power systems (a subject relegated to the retention of synchronism in AC systems). Assuming that stability can be achieved in the energy management system, the next step is to optimize the response according to some performance index. A common performance index for control systems is the integral square error (ISE). The ISE in the *z*-domain is [33]

$$ISE_z = \frac{1}{2\pi j}\oint \eta(z)\eta(z^{-1})z^{-1}dz \tag{2.5}$$

where the closed path of integration is the unit circle and the η function is defined as the difference between the instantaneous value and the final value of the signal, i.e., η is the error.

Normally in a control circuit, the error η would be defined as $\Delta\delta(z)$ in Figure 2.2. However, this is under a paradigm of a control system with a reference value for its feedback. In this typical control scheme, the control assures that the output meets some specification. In the envisioned system, the goal is not necessarily for the load to reach a particular level but to achieve some equilibrium between the pricing signal and the demand. For simplicity, this thesis considers a step in price for the input signal. The system is configured so that after a step in price the load eventually settles at the original nominal level. This assumption allows error to be measure as the value of $\Delta L(z)$ in Figure 2.2. The ISE for the system is demonstrated in Figure 2.3 for demonstration purposes only. The actually data and explanation of the results are discussed in Chapter 4. However, three concepts can be seen in Figure 2.3: 1) there is an initial price step and the price eventually

settles to that initial step value; 2) the load initially responds to the price step and eventually settles to an equilibrium point; 3) the ISE monotonically increases and settles at a value when equilibrium is reached. Therefore, the ISE for a certain input price can be measured by simulation, although it may be limited in its accuracy by the length of the simulation time. In order to minimize the ISE, the simulation can be run for each parameter value. In this case, the feedback gain *B* can be swept and a simulation run for each *B* value.

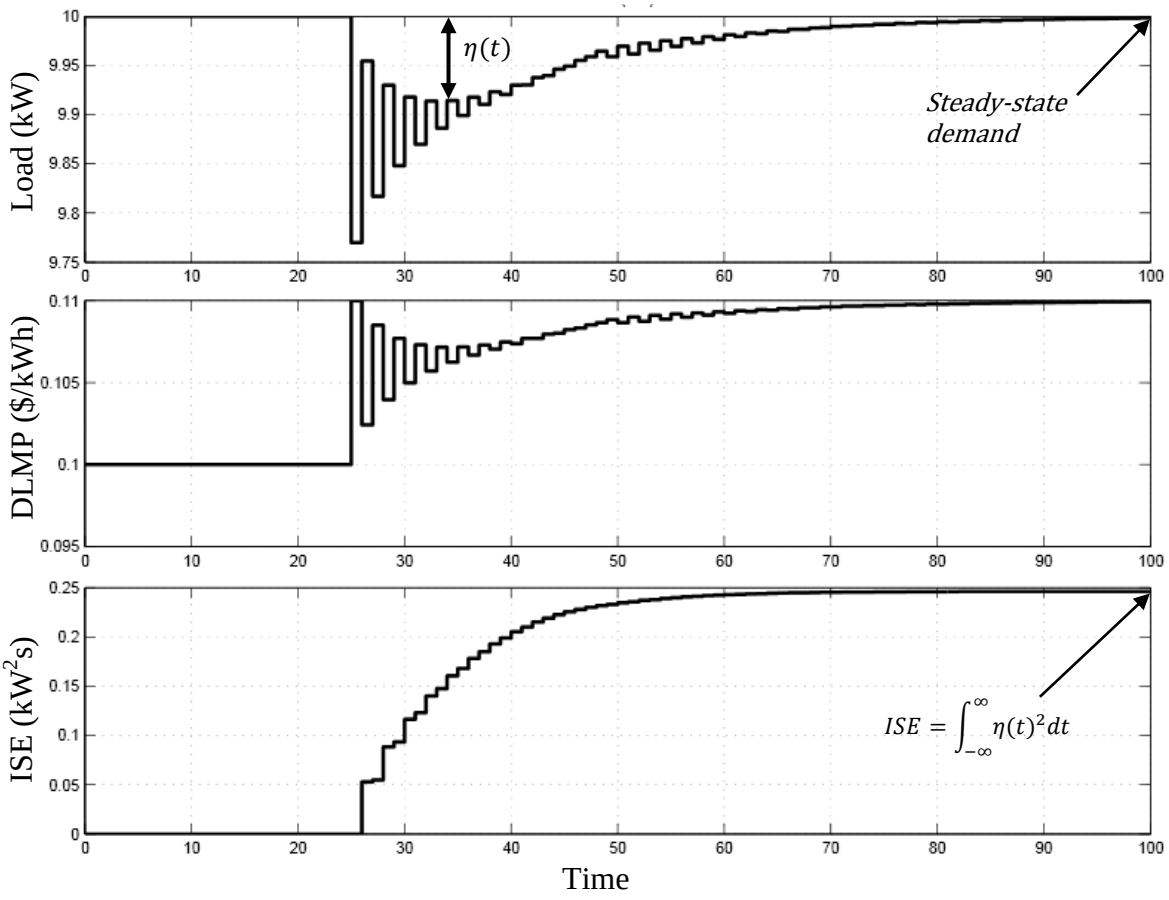

Figure 2.3 Pictorial representation of the integral square error of electric demand in response to a control signal

The ISE can also be calculated analytically for the system in view. In order to change the contour integral of (2.5) into a line integral, a change of variables is made from z to ϕ with the relationship $z(\phi) = e^{j\phi}$,

$$ISE_z = \frac{1}{2\pi}\int_0^{2\pi} \eta\left(e^{j\phi}\right)\eta\left(e^{-j\phi}\right)d\phi. \tag{2.6}$$

Equation (2.6) allows the derivation of the ISE if the η function can be formulated in the z-domain as a function of system parameters and the z variable. In the present application, deriving the η function analytically is non-trivial and specific to the elasticity function. However, when the ISE is calculated analytically, it can be minimized with respect to the parameters of the system (i.e., the feedback gain B in this case).

In the case of parameter uncertainty, instead of minimizing the ISE, robust optimization can be used to minimize the *expected* ISE [55]. In this specific application, the nominal load level is the uncertain parameter and the probability of load $L_{0,i}$ is p_i. The expected ISE is

$$E(ISE(L_0)) = \sum_i p_i ISE(L_{0,i})\,. \tag{2.7}$$

The robust optimization of the ISE with the feedback gain variable is

$$\min_B E(ISE(L_0)) \tag{2.8}$$

where $E(\cdot)$ is the expected value of the ISE computed by

$$E(x) = \int_{-\infty}^{\infty} x p_x(x) dx. \tag{2.9}$$

2.5 Communication of the pricing signal

The pricing signal requires communication between the distribution level control and the controlled loads. The bandwidth of a signal is related to the channel capacity and signal to noise ratio by the Shannon-Hartley theorem [56]

$$C = BW \log_2(1 + SNR) \tag{2.10}$$

where C is the channel capacity in bits/s, BW is bandwidth in Hz, and SNR is the signal to noise ratio. The required communication bandwidth for the pricing signal is estimated by (2.10).

CHAPTER 3

DISTRIBUTED ENERGY STORAGE OPTIMIZATION USING A PRICING SIGNAL

3.1 Introduction

Part of the vision of the FREEDM system is the implementation of energy storage at the distribution level. In order to include distributed energy storage devices (DESD) into the EMS model, some ground work must be laid concerning the control algorithm which determines the power flow into and out of the DESD. The envisioned control of the DESD calculates power flow based on a daily forecast price profile. This chapter investigates the technologies involved in DESD and some of the factors in formulating a battery flow optimization problem. The DESD flows are updated by a real time pricing signal using the concept of a linear price elasticity-based multiplier. In the EMS model, the battery flow is a combination of the nominal flow as solved in the flow optimization problem and a real time response to deviations from the forecasted price.

3.2 Energy storage technology overview

Electric energy storage devices can be used for purposes of power quality, load shifting, power and cost management, and renewable resource integration [57]. The different technologies for energy storage include batteries, supercapacitors, flywheels, pumped hydro, compressed air and thermal storage. The application of an energy storage technology depends partly on what shall be denominated the *duration of discharge*. This is the amount of time that the device is typically used to discharge its stored capacity. Although the duration of the discharge is specific to each application of a technology, a generalized comparison of the durations for different energy storage technologies is shown Figure 3.1. These are by no means precise or definitive time ranges, but show

conceptually what durations might be expected from these technologies. For a more thorough comparison of these energy storage technologies, see [58]. The duration of discharge is related to the potential application of the energy storage device. A very short discharge can help in power quality by discharging energy in sub-cycle time frames. A discharge in the realm of hours can provide load shifting by discharging energy during peak hours and storing energy during off peak hours. Longer-term discharge levels, such as days, can be used for power scheduling [59]. These three categories are shown at the top of Figure 3.1. The EMS envisioned in this thesis uses energy storage to perform load shifting and therefore the battery technology is employed.

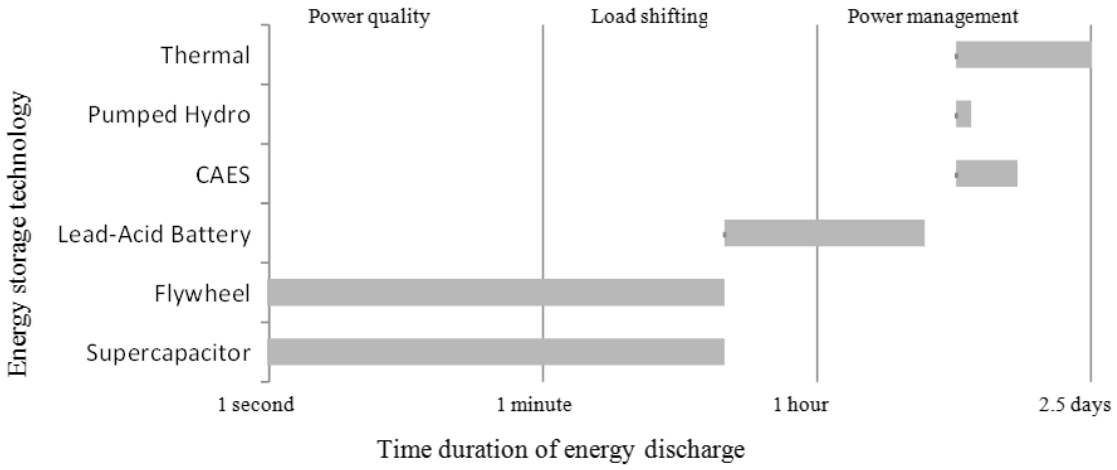

Figure 3.1 Comparison of discharge duration of some commercially available energy storage technologies [60].

Although battery storage is broadly represented by the lead acid battery above, there are many viable alternative battery technologies. In a price controlled system, the cost effectiveness of a battery and its associated rectifier, inverter and controls must be considered. Some technologies for battery storage and their cost-impacting characteristics are found in [61]. This data was used to find a stored energy cost, which is the battery

cost divided by the life-span in cycles. The chart in Figure 3.2 shows the comparison. Since the lead acid battery is both cost effective and a well-established technology, this is used for the present DES study.

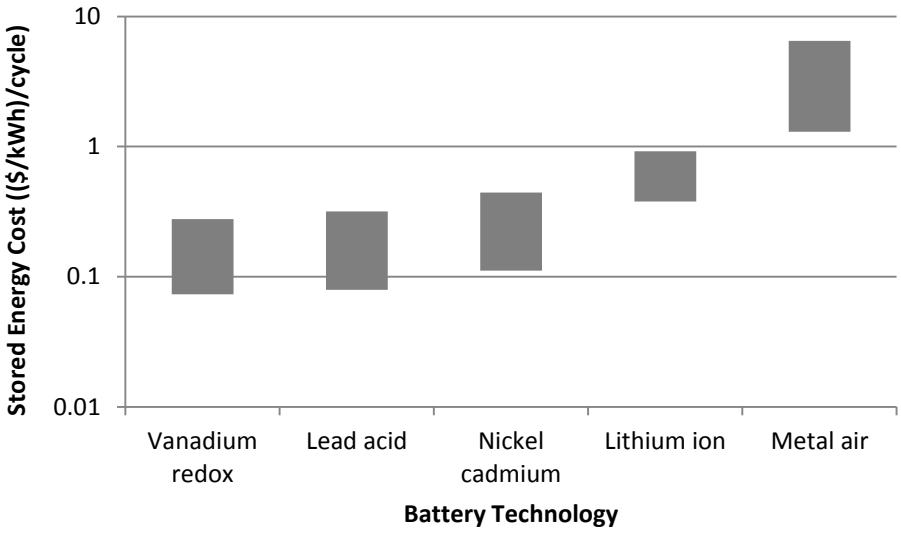

Figure 3.2 The comparative cost for an energy storage cycle for different battery technologies [61].

3.3 Active power losses associated with energy storage

Three losses associated with battery energy storage are considered in this section: distribution system loss, power converter loss and battery loss. The costs associated with these losses are considered simply as the cost to produce the energy absorbed in the losses, although some additional associated costs which are not considered here are discussed in [62-63]. The DESD power flows impact the losses in the distribution system, which could either increase or decrease depending on the layout of the system, the amount power being generated or stored and the location of the DESD [64-66]. The power converter can also be a significant source of loss in battery storage. Some high efficiency converter designs which fall in the range of 2-5% loss are discussed in [67]. Finally, there is power loss in the battery itself. A model for the loss in a lead-acid battery is developed in [68].

The assumption of this paper is that these losses can be estimated as having a quadratic dependence on battery power flow.

3.4 Battery flow optimization objective function

Since a pricing signal is used as a control signal, the DESD can be controlled by the solution to a constrained cost minimization problem

$$\min_{f_n, l_n} \sum_{n=1}^{N} \lambda_n T(f_n + \ell_n) \tag{3.1}$$

where λ_n is the forecasted price of electric energy ($/kWh) at sample n, N is the maximum sample number considered which should account for 24 hours, T is the sample period and f_n is the active power flow into the battery (kW) at sample n. When the cost function is minimized, the cost becomes negative if the cost to store energy ($f_n > 0$) plus the cost of losses is less than the profit from generated energy ($f_n < 0$). The loss ℓ_n is a function of power flow f_n and may include the real power loss (kW) in the power converter, battery and distribution system. The loss function may change depending on the direction of the power flow and therefore the single power flow variable f is broken into two variables: a storage variable s and a generation variable g, such that

$$f_n = s_n - g_n \tag{3.2}$$

where s and g are both positive, active power flows (kW), s into the battery and g out of the battery.

The goal in modeling the losses associated with energy storage is to include the costs of these losses into the objective function of (3.1). In order to make the objective function quadratic, the active power losses in the battery, power converter, and distribution system are modeled as quadratic functions of generation and storage, in the form

$$\ell_g(g_n) = \alpha g_n^2 + \beta g_n + \gamma \tag{3.3}$$

$$\ell_s(s_n) = \chi s_n^2 + \psi s_n + \omega. \tag{3.4}$$

The constants γ and ω partially represent losses that are independent of the level of generation or storage, such as the loss in power electronic equipment which requires a certain amount of power to operate. These constants may also represent a component to the best fit solution to approximate the loss curve of the power electronics, battery, or distribution system. In either case, if the power flow variable is zero, this constant loss should not be included in the total losses, since this represents a loss only associated with a non-zero power flow. This can be represented by adding a binary variable to the loss equation

$$\ell_g(g_n) = \alpha g_n^2 + \beta g_n + \gamma v_n \tag{3.5}$$

$$\ell_s(s_n) = \chi s_n^2 + \psi s_n + \omega u_n \tag{3.6}$$

where v and u are binary variables which represent positive (1) or zero (0) power flow. The objective function of (3.1) can be modified to include the loss formula resulting in a quadratic minimization

$$min_{s,g,u,v} \quad \sum_n c_n T(\, s_n - g_n + \chi s_n^2 + \psi s_n + \omega u_n + \alpha g_n^2 + \beta g_n + \gamma v_n). \tag{3.7}$$

In order to solve (3.7) using *quadratic programming* (QP), [69] demarcates two characteristics that must be met. First, the objective function should be a convex quadratic, meaning that it must fit the form

$$x^T P x + q^T x + r \tag{3.8}$$

where P is a positive semi-definite matrix. The replacement of the multiple variables in (3.7) with the single x variable is done by making x a vector defined as $\begin{bmatrix} s \\ g \end{bmatrix}$, where s and g

are vectors with *N* elements each representing all *N* time periods. For the case of (3.7), *P* is defined by

$$P_{n,n} = \lambda_n T \chi \qquad 1 \leq n \leq N \qquad (3.9)$$

$$P_{n,n} = \lambda_{n-N} T \alpha \qquad N < n \leq 2N \qquad (3.10)$$

$$P_{m,n} = 0 \qquad n \neq m. \qquad (3.11)$$

For P to be positive semi-definite, the diagonals must be positive, meaning α and χ need to be positive, assuming that the price is never negative. The second characteristic of a problem which can be solved using QP is that the constraints must be affine. This leads into the next section establishing the constraints for the battery flow optimization problem.

3.5 Battery flow optimization problem constraints

Assuming that the converter has a maximum power flow and no minimum power flow, the first constraints deal with limiting the generation and storage power flows. The binary variables established in the previous section are accounted for in the constraints to assure that generation and storage are zero in the off state

$$0 \leq g_n \leq v_n P_{max} \qquad \forall\, n \qquad (3.12)$$

$$0 \leq s_n \leq u_n P_{max} \qquad \forall\, n \qquad (3.13)$$

where P_{max} is the upper limit of active power flow through the power converter. The second constraint assures that the battery is not simultaneously in a state of charge and discharge

$$v_n + u_n \leq 1. \qquad \forall\, n \qquad (3.14)$$

The final constraint is that the energy storage must not exceed the battery capacity on the upper bound or the minimum battery charge on the lower bound,

$$B_{min} \leq \sum_{n=0}^{k} T(s_n - g_n) \leq B_{max} \qquad \forall\, k \qquad (3.15)$$

where B_{max} and B_{min} are the maximum and minimum allowable charge in kWh for the battery. An additional constraint is required to balance battery charge and discharge through an optimization period. It is assumed that for any period considered, the battery needs to charge and discharge an equal amount. Therefore, if the time period begins with an initial charge in the battery, it must end with the same amount of charge stored in the battery,

$$\sum_{n=0}^{N} T(s_n - g_n) = 0. \qquad (3.16)$$

Since all of the above constraints are affine, QP can be used to solve the formulated battery flow optimization problem.

3.6 Further characterization of the battery flow optimization problem

The battery flow optimization problem is envisioned providing a power flow profile using a forecast of real time energy prices. In the interest of this thesis, the battery is envisioned using near full capacity and providing a continuous power flow profile which can be approximated by the linear model of the system. Since cost minimization is not the sole objective for energy storage, an additional objective function shall be added to the optimization problem. Multi-objective programming (MOP) is a method of optimizing over multiple objective functions. The general form of a MOP composite objective function is *I(x)*

$$I(x) = w_1 c_1(x) + w_2 c_2(x) \tag{3.17}$$

where w_1 and w_2 are weights for each objective (cost) function. There are several approaches to the constrained multi-objective optimization problem. This problem might be solved using the normal boundary intersection (NBI) method [70]. There are alternative formulations of the multi-objective optimization problem, some of which are discussed in [71-76]. In the present application, the indicated multi-objective optimization methods are deferred in favor of a straightforward heuristic approach. The approach used is to fix one weight and select the other weight for operational convenience. More specifically, w_1 may be set to unity in order to determine only w_2 since only the ratio of the weights impacts the solution in this case. The first cost function c_1 in (3.17) is taken to be the cost function represented in (3.7). The second is a penalty for 'extreme' generation or storage levels. That is, c_2 is used to reduce large levels of power flow and incentivize smaller, more even levels of net demand. Therefore, an appropriate objective function is the Euclidean norm of the power flow variables indicated in (3.16),

$$\|s + g\|_2^2. \tag{3.18}$$

In order to determine w_2, the shadow price of the battery capacity constraint (3.15) denominated μ_{cap} is used. This shadow price is non-zero when the battery reaches a state of full charge and is neither being discharge nor charge. If the battery reaches a state of full charge, it may not respond to price changes. This creates a potential non-linear response to price that must be eliminated. Therefore, the criterion $\mu_{cap} = 0$ for all k is used for the verification of w_2, as seen in Figure 3.4.

3.7 Battery demand price elasticity

Ultimately, the battery flow control algorithm needs to produce two things: 1) a nominal flow profile and 2) a linear multiplier to adjust the flow to real time price deviations. The nominal flow profile is solved by the multi-objective optimization problem, i.e., the solution to (3.17). In order to assign the linear multiplier, the concept of price-elasticity is combined with the shadow price associated with the balance of charge constraint in (3.15). This shadow price is the value of the next kWh of energy storage capacity. As a linear estimate, it is approximated that every kWh of stored energy is worth this amount. The self-price elasticity can, therefore, be approximated using this shadow price

$$E_{Sn} = -\frac{\lambda_n}{\lambda_n - \mu_{ch}} \qquad \forall\, n \qquad (3.19)$$

where μ_{ch} is the shadow price for the charge balance in (3.16), λ_n is the cost as sample n and E_n is the self-price elasticity of the battery flow at sample n. The concepts of this paragraph are demonstrated in Figure 3.3. Therefore, power does not flow from the battery when the price is at μ_{ch}, flows into the grid above μ_{ch}, and flows from the grid when the price is below μ_{ch}.

3.8 Optimizing with the MOSEK solver

The chosen solver for the battery flow optimization problem is MOSEK [77]. Some popular solvers are discussed and compared in [78]. A difficulty with finding the shadow price μ_{ch} for use in the elasticity formula (3.19) is that the MOSEK solver cannot produce shadow prices for problems with binary variables [77]. Two solutions exist to this problem. First, the binary variables could be eliminated altogether. This is an appeal-

ing solution, since the computation requirements increase considerably when binary variables are included. However, this does not most accurately represent the battery costs.

The second solution is that a second optimization problem could be created which is identical to the first except that the binary variables are set to the solutions from the first optimization problem. In this case, the binary variables would now be constants and therefore the second iteration would be able to produce shadow prices. The flow chart for the optimization problem solving process is shown in Figure 3.4. Note that the program CVX was used to interface between Matlab and the MOSEK solver [79].

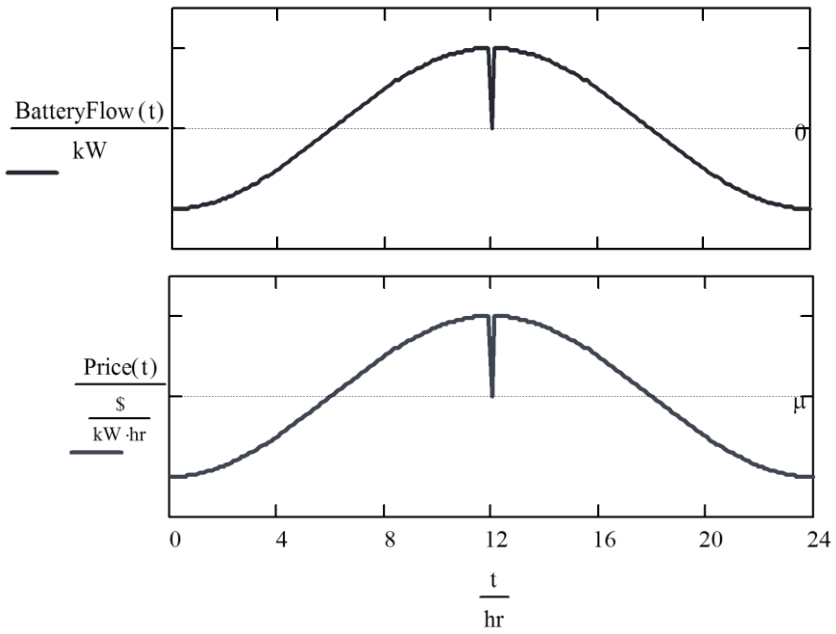

Figure 3.3 A pictorial representation of the relationship between the battery power flow, the electric energy price and the shadow price μ_{ch}.

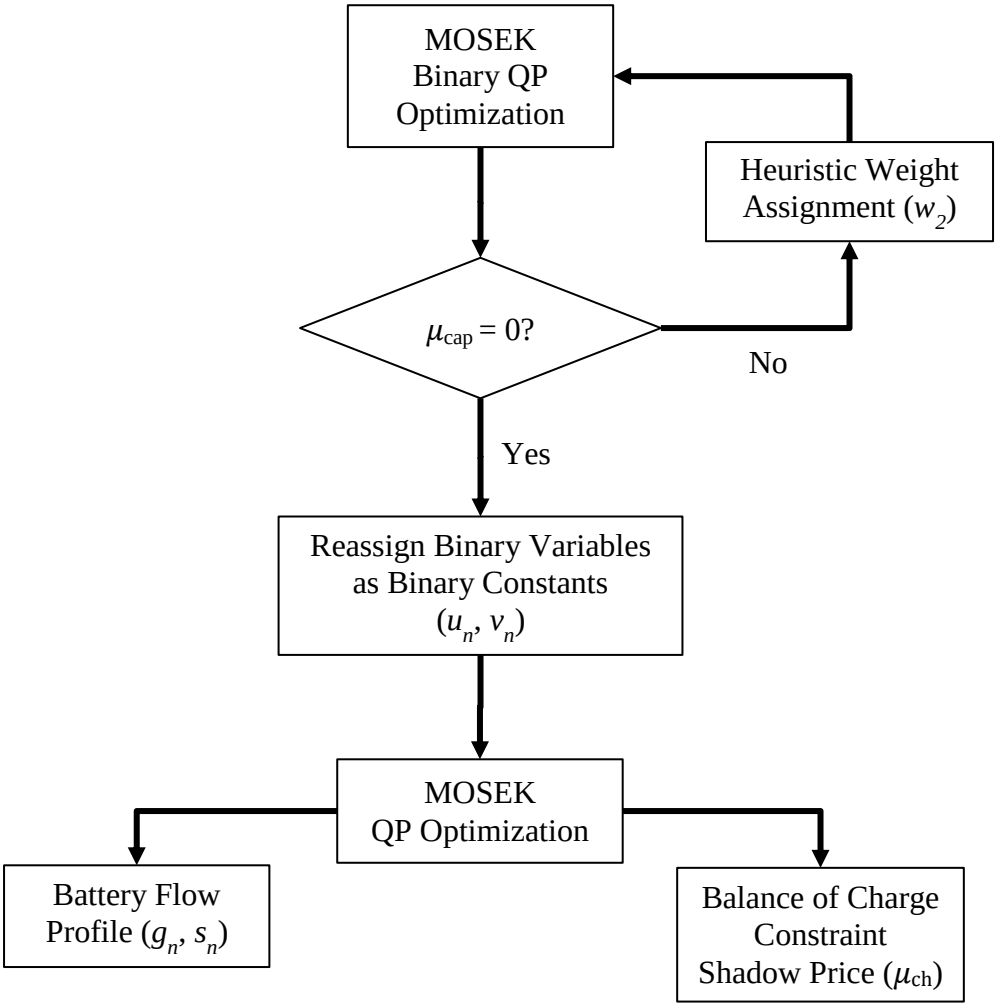

Figure 3.4 Flow chart for the battery flow optimization procedure.

CHAPTER 4

PRICING BASED CONTROL OF THE FREEDM SYSTEM: ILLUSTRATIVE CASES

4.1 Introduction to the use cases

The preceding chapters presented a price based control for the FREEDM distribution system. In this chapter, five use cases are presented to illustrate the proposed control. In each case, stability and ISE are determined using a distribution level pricing signal as an input and a load control output signal. The model in the *z*-domain is shown in Figure 4.1. The BIBO stability of the system is determined by the small signal transfer function

$$H(z) = \frac{\Delta L(z)}{d(z)} \tag{4.1}$$

where the input signal is $d(z)$ and the output signal is $\Delta L(z)$. The parameters L_0, E_S and δ_0 are considered constants in order to render the system linear. The feedback gain B is 'swept' during the system performance evaluation and analysis. The five use cases are:

- Use case 1 – single input single output (SISO) configuration used as a base case
- Use case 2 – the same SISO configuration as use case 1 but with a different cross-price elasticity function
- Use case 3 – multiple input multiple output (MIMO) configuration with two distribution level price signals and two distribution load outputs
- Use case 4 – single input multiple output (SIMO) configuration with a single price and a single distribution node, but with battery energy storage as an additional load

- Use case 5 – the same SISO configuration as use case 1 but with uncertain load.

These scenarios are explained further in their respective subsections. The goal of analyzing these two scenarios is to illustrate how the different parameters of the price controlled system affect the BIBO stability and the ISE performance.

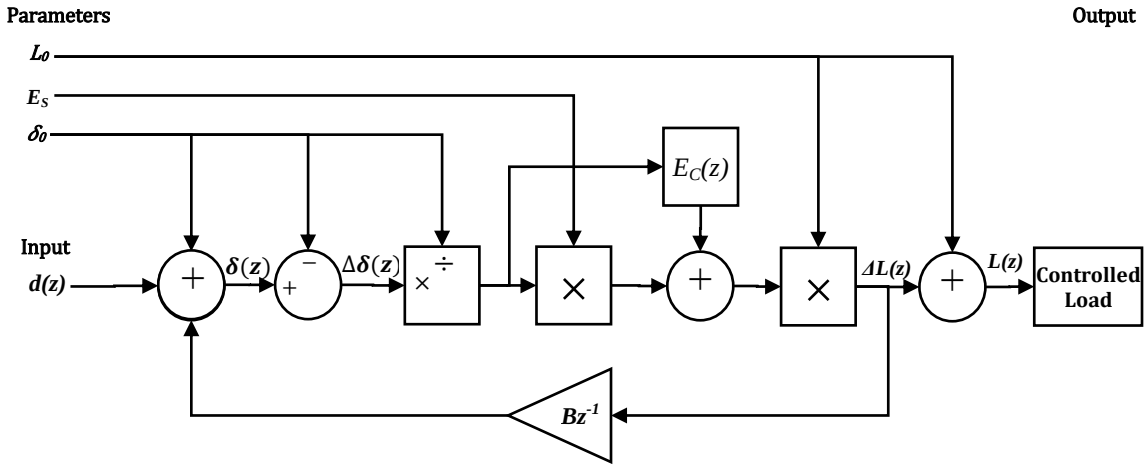

Figure 4.1 Distribution EMS system under consideration illustrative use cases.

4.2 Use case 1: single input single output system base case

In this first use case for the price controlled EMS, the circuit shown in Figure 4.1 is analyzed as a base case for comparison with the other use cases. Use case 1 is also used to illustrate the basic functioning of the price controlled system. It uses a formula which creates constant cross-price elasticity for a set number of samples,

$$E_C(z) = -\frac{E_S}{N-1}\sum_{n=1}^{N-1} z^{-n} \qquad \text{for } n = 0,1,\ldots N\text{-}1$$
$$E_C(z) = 0 \qquad \text{for } n \geq N. \tag{4.2}$$

In (4.2), $n = 0$ begins the count of samples at the time of the price change and *N-1* is the total number of future samples considered for cross-price elasticity. The equations in

(4.2) essentially state that for all the considered time samples *N-1*, the cross-price elasticity is a constant. Note that the sum of all the price elasticity multipliers is zero in conformity to (1.6). The cross-elasticity goes to zero *N* samples after the price change. That is, a change in price only directly impacts the load up to *N* samples after the price change occurs.

There are two tracks that the analysis of this circuit takes. First, a discrete model is created in Simulink in order to demonstrate the operation of the control system and to minimize ISE. Then, an analytic model of the system transfer function is derived to perform BIBO stability analysis and ISE minimization. The ISE of the Simulink model is compared with the formulaically calculated ISE to demonstrate the use of the ISE analysis using the Simulink model.

The SISO system for use case 1 was created in Matlab Simulink and can be viewed in detail in Appendix A.3. In order to demonstrate the working of the system, a single-sample pulse is used as the input signal *d(z)*. This pulse raises the DLMP by 10% for one sample period. Any additional changes in the DLMP occur as a result of feedback. The load and price signals which result from this pulse input are shown in Figure 4.2 for three different feedback gains. When the feedback gain is zero, note that the initial reduction in the load level is determined by the self-price elasticity and is due to the temporary rise in price. The subsequent rise in load level is due to cross-price elasticity and compensates the energy lost during the momentary high price. When the feedback gain is positive, the price pulse causes an oscillatory effect of alternating price and load levels. When the feedback gain is sufficiently high, the system produces an unbounded signal output.

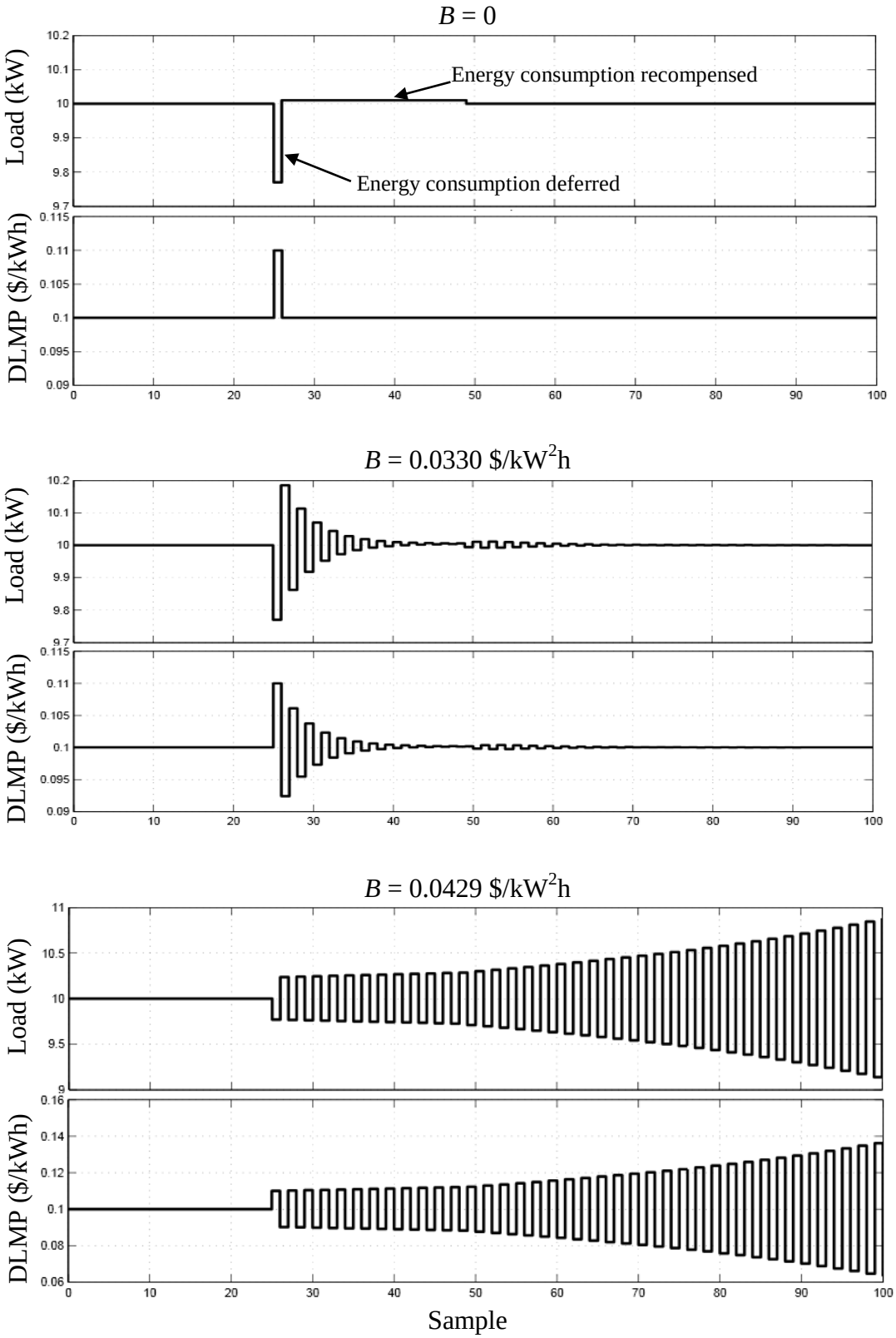

Figure 4.2 Demonstration of use case 1 signal responses to a price impulse.

The system model in Figure 4.1 was also analyzed formulaically to illustrate the BIBO stability and ISE dependence on the feedback gain. The analytic derivation of the transfer function *H(z)* begins with the derivation of the equations for the discrete time signals. The formula for the real time DLMP signal is

$$\delta(z) = \frac{\delta_0}{1-z^{-1}} + d(z) + Bz^{-1}\Delta L(z). \tag{4.3}$$

The load is adjusted with a small-signal load update $\Delta L(z)$ defined by

$$\Delta L(z) = L_0 \frac{\delta(z) - {\delta_0}/{1-z^{-1}}}{\delta_0}\left(E_S - \frac{E_S}{N-1}\sum_{n=1}^{N-1} z^{-n}\right). \tag{4.4}$$

The input signal *d(z)* and the output signal $\Delta L(z)$ are isolated and the transfer function of (4.1) is derived by the ratio of the two. This transfer function, *H(z)*, has a polynomial numerator and denominator, both of the order *N*+1, and was derived using Mathcad symbolic analysis tools, as seen in Appendix A.1. The analytic derivation of *H(z)* was used to find the poles for a few values of the feedback gain *B*, seen in Figure 4.3. Note that when the feedback gain increases, the negative real axis pole crosses the unit circle, signifying that the system is not BIBO stable.

The integral square error was also derived for use case 1. In order to find the ISE, the final value must be known in advanced to know the error of the signal. A step function is used as the input signal *d(z)* to analyze the ISE. For a step in the distribution LMP and a constant nominal load, the final load power level is the same as the initial load level, since the sum of the cross-price elasticity multipliers in the brackets of (4.2) is equal to the negative of the self-price elasticity, in accordance with (1.6). Therefore, any change in load level can be considered error for a step price input. The ISE was derived analytically in Mathcad and these formulas are in Appendix A.2.

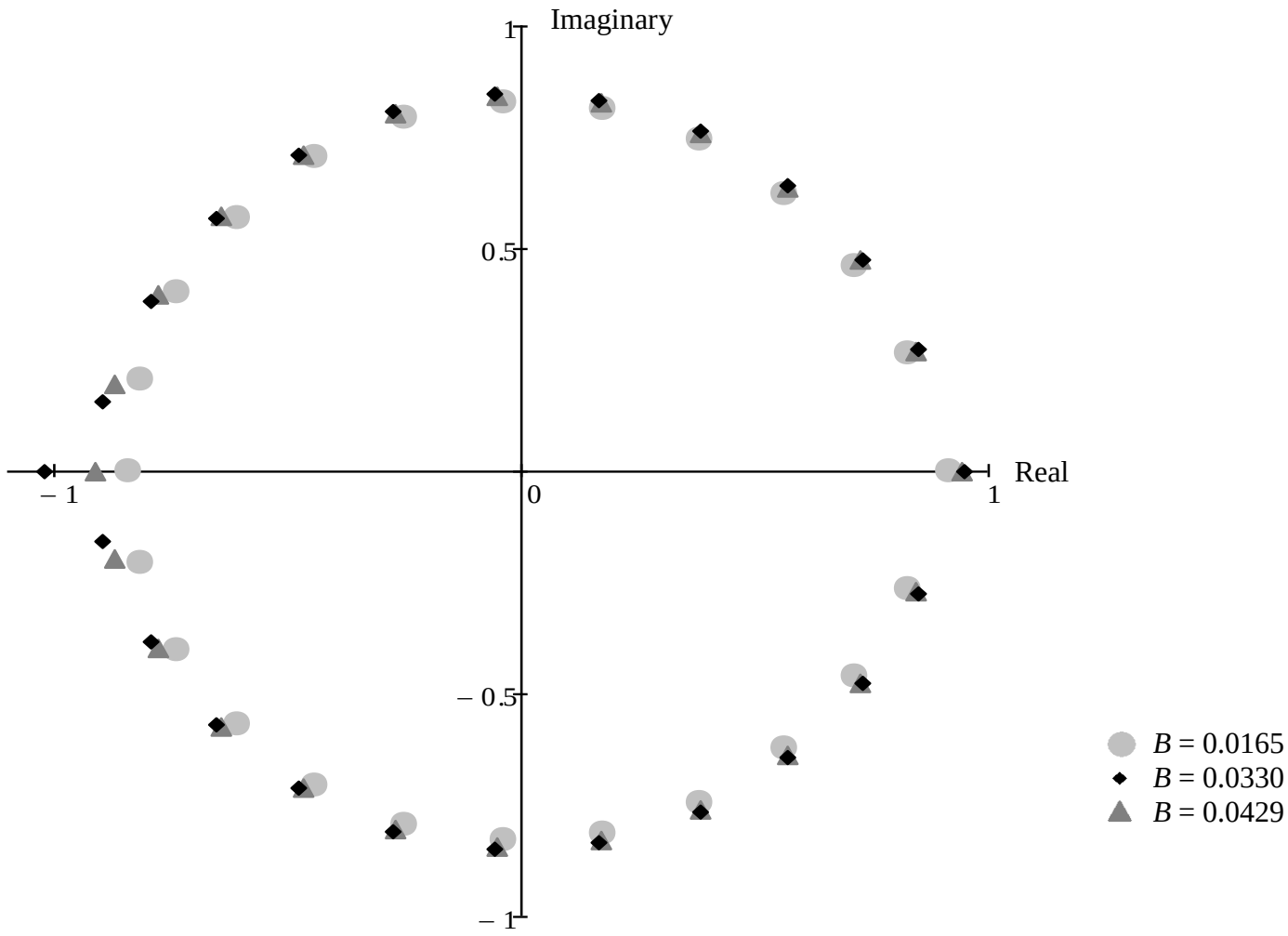

Figure 4.3 SISO *z*-domain transfer function pole locations for constant E_C with three feedback gain values.

The ISE was minimized over a sweep of the *B* parameter with the optimal *B* considered as the value which resulted in the minimum ISE. These results are shown in Figure 4.4. The same analysis was performed in Simulink and the results are similar. However, since the simulation in Simulink cannot be performed for infinite time, the integral for the ISE becomes increasingly inaccurate as oscillations in the output signal continue for longer times. The graph for the ISE as calculated in the Simulink model can be found in Appendix A.3.

The goal of the use case 1 illustration is to demonstrate the basic functioning of the pricing signal controlled EMS and to present a base case for comparison with other use cases. The next four cases change different system parameters to illustrate their effects on performance.

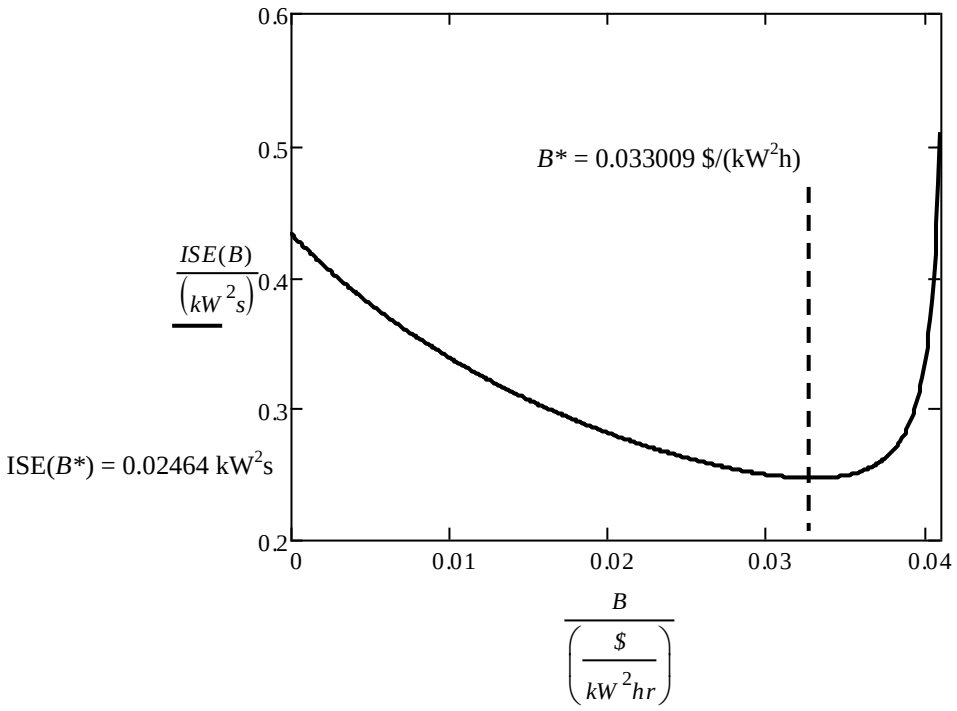

Figure 4.4 ISE minimization for the SISO system under use case 1.

4.3 Use case 2: alternate cross-price elasticity formulation

The second use case for the SISO system of Figure 4.1 considers a cross-price elasticity which decreases linearly over time. The sum of the self-price elasticity and all the cross-price elasticity multipliers is zero in conformity to (1.6). Compared to use case 1, this use case represents a method of more rapidly restoring much of the energy deferred by a rise in price. The cross-price elasticity as a function of the sample number is

$$E_{C_n}(z) = -E_S\left[\frac{2}{N-1} - n\frac{2}{N(N-1)}\right]z^{-n} \qquad \text{for } n = 0,1,\ldots N-1.$$
$$E_C(z) = 0 \qquad \text{for } n \geq N \tag{4.5}$$

The cross-price elasticity multiplier in the brackets in (4.5) decreases as the samples move forward in time from the initial price change. By the N^{th} sample, the cross-price multiplier reaches zero and remains zero.

The formula in (4.5) is used to derive an analytic expression for the transfer function for use case 2. The DLMP signal formula is that given in (4.3) but the load update signal changes to

$$\Delta L(z) = L_0\frac{\delta(z) - {\delta_0}/{1-z^{-1}}}{\delta_0}\left(E_S - E_S\sum_{n=1}^{N-1}\left[\frac{2}{N-1} - n\frac{2}{N(N-1)}\right]z^{-n}\right). \tag{4.6}$$

The transfer function *H(z)* is derived for use case 2 and the poles are plotted for various feedback gain values, presented in Appendix A.4. The integral squared error is plotted as a function of the feedback gain *B* in Figure 4.5 and the derivation of the ISE in Mathcad is in Appendix A.5. The ISE analysis was repeated using Simulink with similar results in Appendix A.6. The minimum ISE was found to be 0.0175 kW^2s for B^* = 0.0302 $/($kW^2h$).

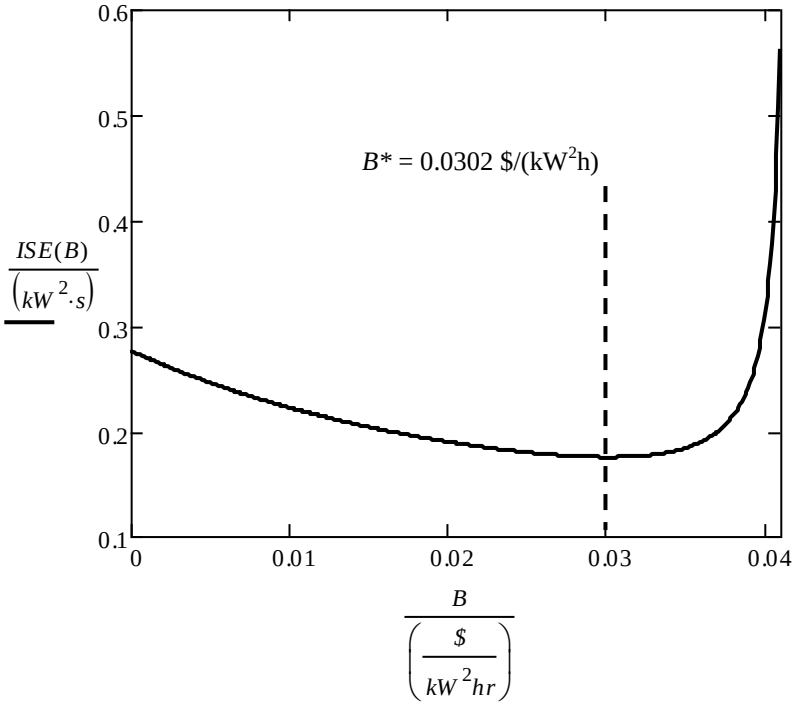

Figure 4.5 ISE minimization for the SISO system under use case 2.

The comparison between the results in Figure 4.4 and the results in Figure 4.5 show that the cross-price elasticity function influences the performance of the system. The cross-price elasticity function represents the type of response the load has to a price change. If the load attempts to spread out the recovery of energy lost in a price increase, the optimal feedback gain is relatively higher and the ISE is lower. If the load attempts to recover the lost energy more quickly, the optimal feedback is lower.

4.4 Use case 3: multiple input multiple output system

The first use case involved a system with a single load which was influenced by a single price input signal. However, the distribution system in view for FREEDM consists of many distribution nodes, each responding to a locational pricing signal specific to that node, with the power demand at each node potentially influencing the price at the other

nodes. With multiple nodes in the distribution system, the interdependency between power demands *via* the DLMP pricing signal is represented as a multiple input multiple output (MIMO) control system. The block diagram in Figure 4.1 is used, but for use case 3 the signals indicate vectors of k elements for the k distribution nodes. The following analysis considers the case for two distribution nodes, i.e.; $k = 2$. Addition, subtraction, division, and multiplication blocks of Figure 4.1 all perform their operations element-wise. The feedback gain B can be broken into a matrix of gains between the load change at one node and the price change at each other node, where the elements in the B matrix

$$B_{j,k} = \frac{\partial \delta_j}{\partial \Delta L_k}. \tag{4.7}$$

The input signal for the MIMO system analysis is the pricing signal for distribution node 1 and the output signal is the load at node 1,

$$H_{11}(z) = \frac{\Delta L_1(z)}{d_1(z)}. \tag{4.8}$$

The ISE analysis is performed in Simulink for sweeps of B values. The assumption for the B matrix is that $B_{11} = B_{22}$ and $B_{12} = B_{21}$. The circuit and code for this simulation can be seen in Appendix A.7. The plot of ISE values for multiple B_{11} and B_{12} values is shown in Figure 4.6. Note that the ISE is minimized at $B_{12} = 0$, which means that the price at one node is not impacted by a load change at another node. Since the demand at one node of a distribution system can impact the cost of delivering energy to another node in a distribution system, there may be economic reasons for B_{12} to be nonzero. That is, a nonzero B_{12} might more accurately reflect the costs of energy delivery. Nevertheless, a nonzero B_{12} increases the ISE for the price control of the load. The minimum ISE here is 0.2464 kW^2s, the same as in use case 1.

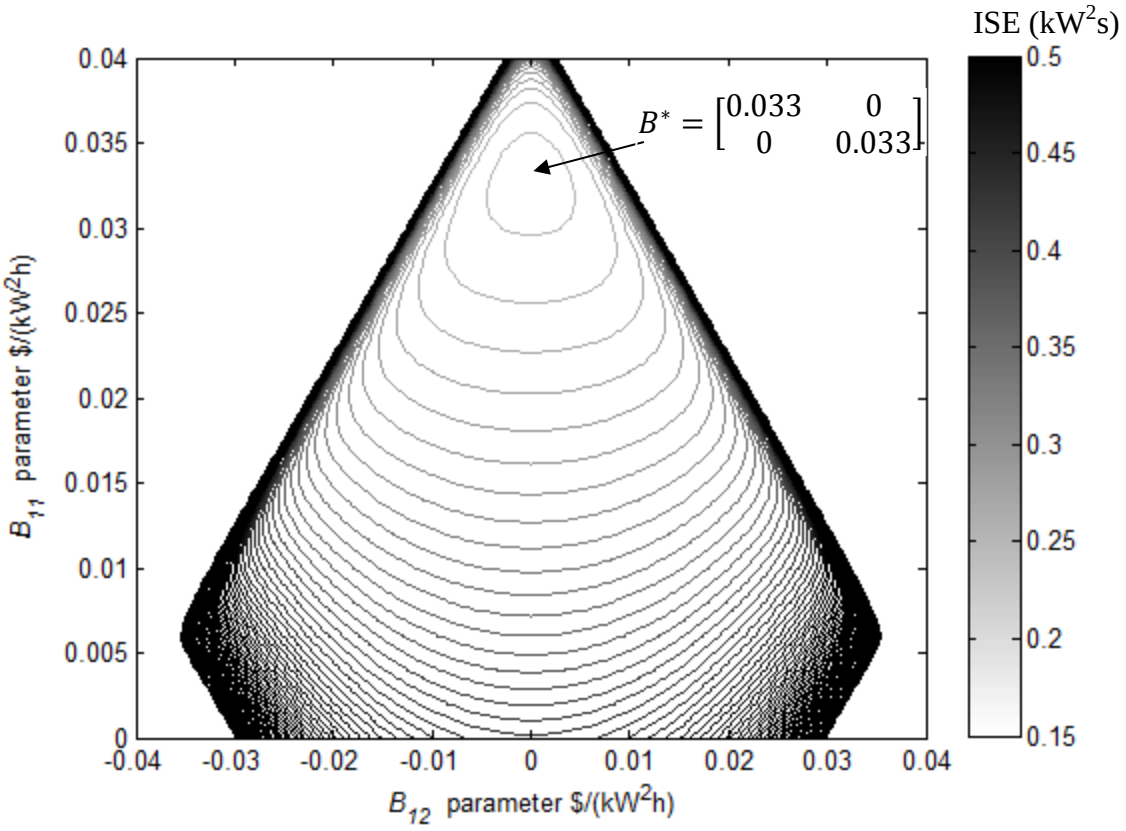

Figure 4.6 ISE minimization for use case 3.

4.5 Use case 4: single input multiple output with DESD

The previous use cases assumed a distribution level load which had price elasticity less than unity. This is considered a *price inelastic* demand and is in line with the results of demand response program studies which are reviewed in Chapter 1. However, in the envisioned FREEDM distribution system, the loads include distributed energy storage. The price elasticity of energy storage may have an impact on the performance of the EMS system since a small change in price may very well result in a large change in power flow requested by the DESD. That is, demand for DESD may be very *price elastic*. A battery flow optimization was performed for a 5 kWh lead acid battery as seen in Appendix A.8 and the operation at peak price was found to be 0.67 kW power generation with a

self-price elasticity of 297%. The battery was included in parallel with a 10 kW load from use case 1, creating a single input multiple output (SIMO) system. The ISE was optimized for the SIMO system with a distribution level load and battery both controlled by the same pricing signal and the results are shown in Figure 4.7. Although this battery generates less than seven percent of what the load consumes, due to its large price elasticity it almost cuts the optimal feedback gain B in half. Therefore, the DESD restricts the values of B which result in a BIBO stable system, as compared to use case 1. The ISE remains 0.2464 kW^2s.

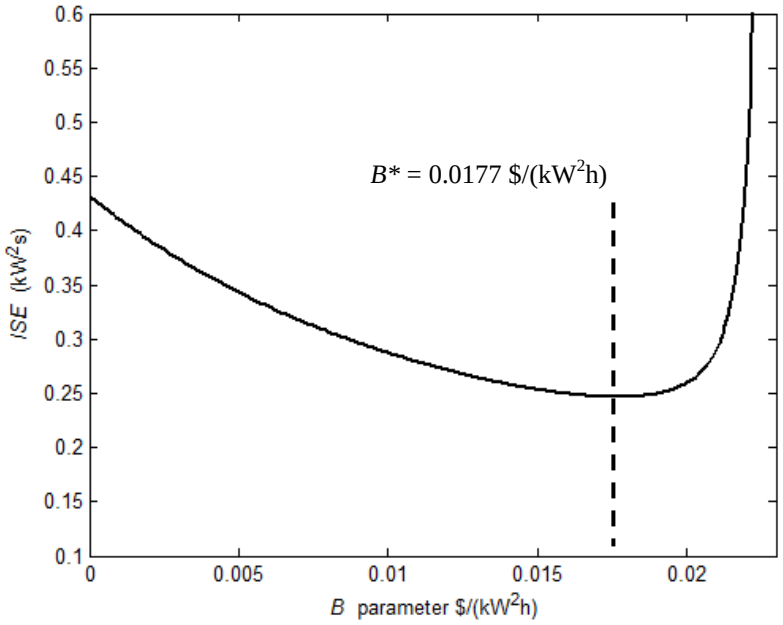

Figure 4.7 ISE minimization for the SIMO system for use case 4.

4.6 Use case 5: single input single output with uncertain load

In the previous ISE minimizations, the nominal load was considered a known value. In implementation, the load may be uncertain. Load variation could cause a problem due to a combination of two phenomena. First, the 'optimal' B to minimize ISE may be dependent on the load level. Second, the slope of the ISE curve increases rapidly when B

> B^*, as in Figure 4.4. The strategy for use case 5 is to select B for several different nominal load levels and weight the resultant ISE calculations using the probability of those given load levels. This is an example of *robust optimization*. In all cases, the B selected must render the system BIBO stable. For the present application, to implement robust optimization a probability distribution was assigned to the load level. A Gaussian distribution was used for the load level in this demonstration, but a more realistic distribution could be used if it were available. For use case 5, the load was modeled as Gaussian with discrete load levels with a mean of 10 kW and a standard deviation of 1.0 kW, shown in Figure 4.8. The load level distribution was used in simulation in Appendix A.9 to find the expected value of the expected ISE for each value of B seen in Figure 4.9. Note on this figure that the expected ISE rises steeply above optimal B. This is the effect of an unbounded output, which results in an infinite ISE. Any load which causes an unbounded output will thus result in infinite expected ISE according to (2.7) The results of use case 5 are a robust B^* of 0.0294 \$/(kW^{2}h) and a corresponding expected ISE of 0.2541 kW^{2}s.

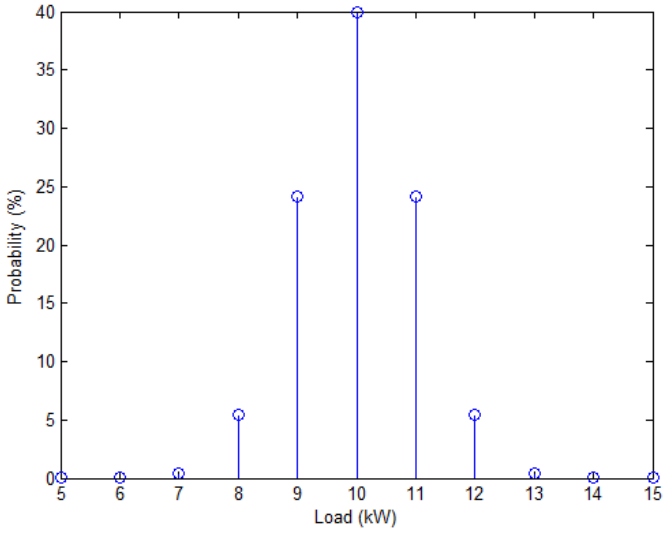

Figure 4.8 Probability density for the robust optimization in use case 5.

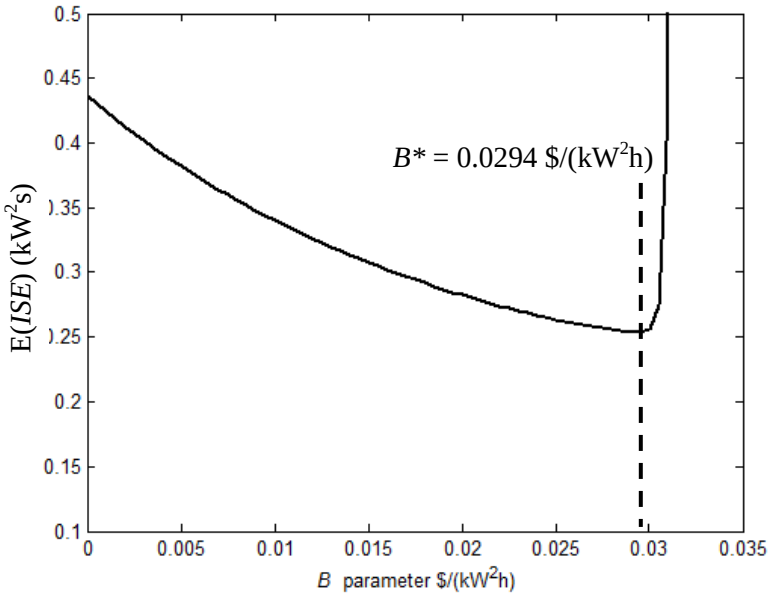

Figure 4.9 ISE minimization for the SISO system for use case 5.

4.7 Summary of use cases

Use cases 2-5 implemented four scenarios for the price controlled EMS to compare to use case 1. Optimal feedback gain B^* and minimum ISE for each use case is shown in comparison to use case 1 in Figure 4.10. In the diagram, the numbers in each box are the use case numbers. Other system parameters were varied and the results can be seen in Table 4.1. Use case 1 for these comparisons is use case 1 parameter values, which can be found in Appendix A. These illustrations suggest that the price controlled system in view can use the feedback gain to assure stability and minimize ISE in practical operation in one of three ways:

1) The calculation of B^* could be *updated* as the system parameters change. This strategy could be supported by the increased level of communication which is envisioned in the Smart Grid. Loads could update their power consumption levels, self-price elasticity, and cross-price elasticity characteristics to allow an operational real time B calculation.

2) The system parameters could be *limited* to maintain bounded output for a fixed *B*. The consumer price elasticity and power consumption could be limited. However, limiting all parameters which affect performance would necessarily limit the initial forecast DLMP. This option moves away from the market equilibrium envisioned.

3) There could be some *combination* between the first and second options. Some parameters could be limited while others are allowed to vary. This would require proper communication of these parameter values in order to calculate *B**.

Table 4.1 Parameters of the SISO system and their respective impacts on *B** and ISE.

Parameter change	Impact on *B**	Impact on minimum ISE
E_S increase	Decrease	Increase
$d(z)$ step size increase	Same	Increase
L_0 increase	Decrease	Increase
δ_0 increase	Increase	Decrease
$E_C(z)$ weighted more toward recent samples	Decrease	Increase

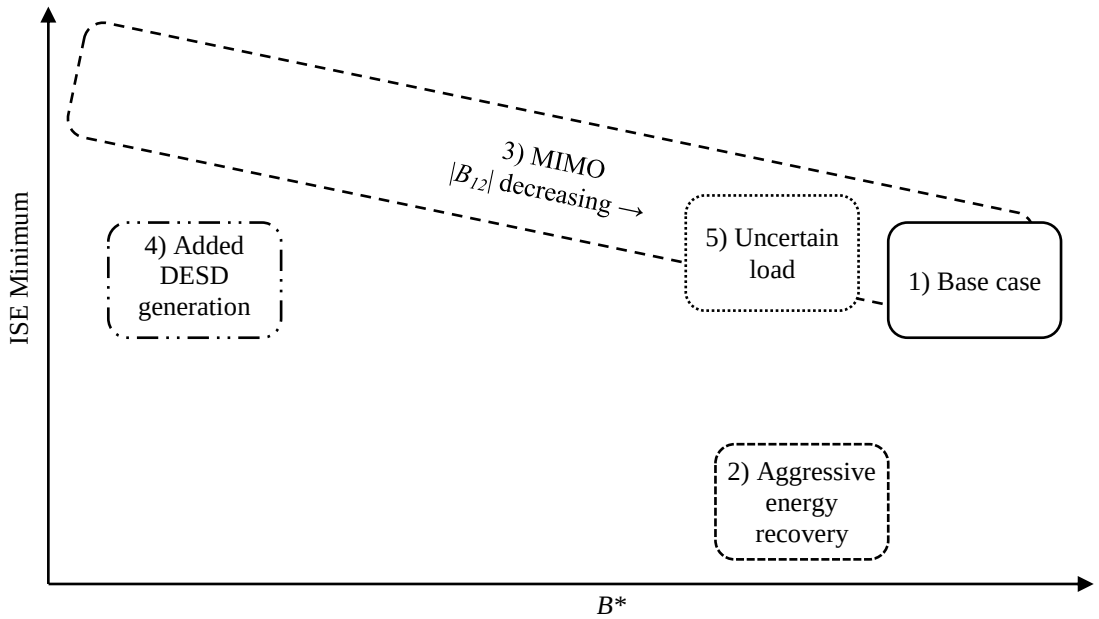

Figure 4.10 Relative effects of parameter changes to the price controlled EMS.

4.8 System communication requirements

The communication of a price signal and of parameter values or limitations requires a communication infrastructure. The envisioned channels are shown in Figure 4.11, where parameter values of the load are considered consumer 'preferences' and parameter limitations are labeled 'response limitations.'

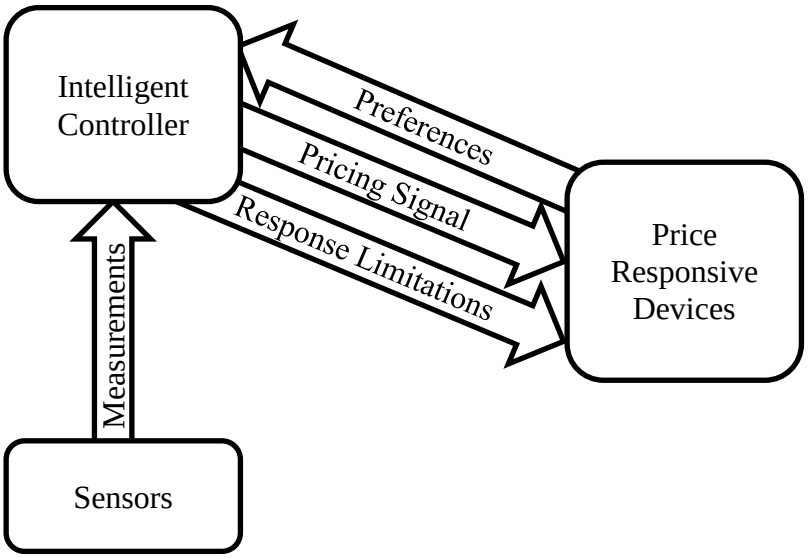

Figure 4.11 Communication channels envisioned in the price controlled EMS.

The illustrative use cases used a pricing signal updated every second. If the precision of the price is nine decimal places, this corresponds to 32 bits per second. The theoretical bandwidth of this system from (2.9), assuming a signal-to-noise ratio of 200, is about 4 Hz. In the system in view, a more rapid control may be desired. If the pricing signal updates every 4 milliseconds, the bandwidth increases to 1.046 kHz. Figure 4.12 illustrates the variation in the communication bandwidth for a 200 signal-to-noise ratio, 32 bit technology versus sample time. Note that this bandwidth is only for the communication of the pricing signal itself. Any additional communication in the system may re-

quire more bandwidth. This is especially true for any communication parallel to the communication of the pricing signal, including customer response limitations or customer preferences.

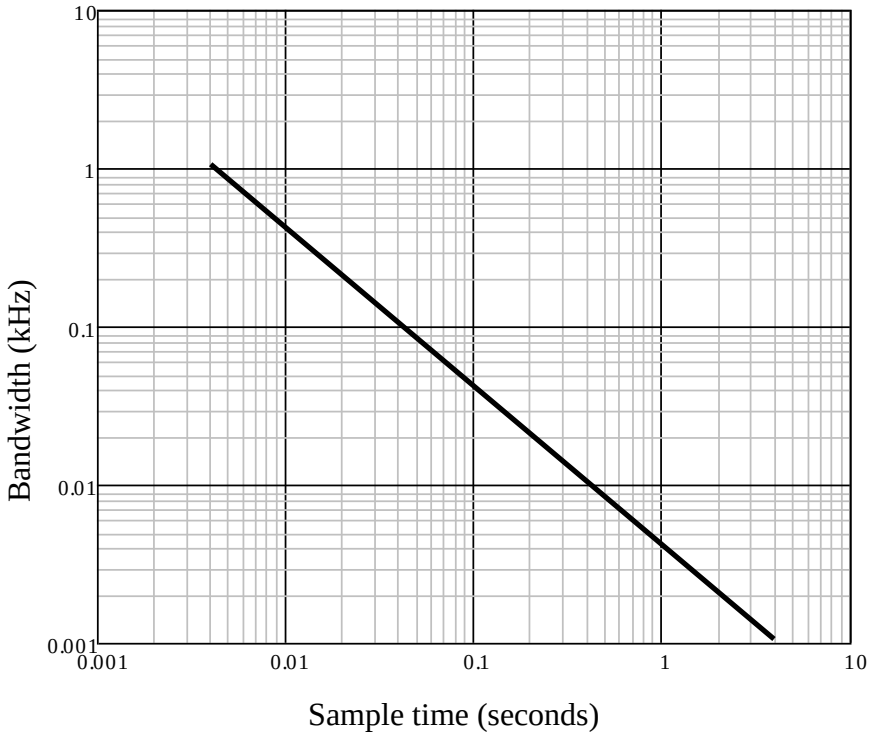

Figure 4.12 Relationship between the sample time and badwidth of a pricing signal for an energy management system.

CHAPTER 5

CONCLUSIONS AND FUTURE WORK

5.1 Conclusions

This thesis concerns a distribution class LMP pricing control signal for load management in the FREEDM distribution system. The control system was analyzed using a small-signal, linear *z*-domain model. The transfer function between the pricing signal and the load response was evaluated for bounded input, bounded output stability and integral square error. The BIBO stability of the system was shown to depend on the feedback gain between the change in load and the price. If the price responded too aggressively to load changes, the output signal of the system controlling the load became unbounded. The integral square error was used as a performance index to evaluate the control system. Five use case illustrations demonstrated that the ISE was impacted by the system parameters. In each case, the pricing signal was given a 10% price step and the ISE of the load control signal was evaluated. The feedback gain was optimized to find the minimum ISE. The following main conclusions are made from these cases:

- Load management can be achieved by use of a pricing signal in a power distribution system.
- The response of the load to a pricing signal can be modeled in a linear control system using the price elasticity of the load energy demand.
- The price controlled system has BIBO stability issues which can be alleviated by appropriately designing the parameters of the system.
- The theoretical bandwidth required for a pricing signal was determined to be on the order of 1 kHz for a 4 millisecond pricing update period. Other

potential communication requirements exist and depend on the implementation of the system.

- The indicated pricing based feedback configuration appears to be well suited for electronically controlled power distribution as used in the FREEDM system.

Each of the five cases also demonstrated more specific information regarding the use of a pricing signal as a control for energy management:

- Use case 1 was a single input and single output system and demonstrated that the load could be controlled by a pricing signal. The BIBO stability and ISE was affected by the feedback gain. For use case 1, the 'optimal' feedback gain was 0.033 \$/(kW^{2}h) and the ISE was 0.2464 kW^{2}s.

- When the cross-price elasticity more rapidly compensated for deferred energy in use case 2, B^* slightly dropped to 0.030 \$/(kW^{2}h) and the ISE fell to 0.1747 kW^{2}s.

- Use case 3 illustrated a system with two loads, two pricing signals and feedback gain between the loads and pricing signals. The optimal feedback gain between the load control signal and the pricing signals for *other* loads was B_{12}^*= 0. This resulted in an optimal operation at the same point as use case 1, where B_{11}^* = 0.033 \$/(kW^{2}h) and ISE = 0.2464 kW^{2}s. If economic reasons compel the operator to make $B_{12} > 0$, the ISE rises and the B_{11}^*drops.

- Energy storage was included in the system in use case 4, creating a single input dual output system. The large price-elasticity of the battery storage creates BIBO stability issues. A single 5 kWh battery was used and this reduced B^* to 0.0177 \$/(kW^{2}h). The ISE remained the same as in use case 1.
- Use case 5 optimized the expected ISE for an uncertain load demand level. Using *robust optimization* and an assumed load level probability distribution, B^* was 0.029 \$/(kW^{2}h) and the expected ISE was slightly higher than use case 1 at 0.2541 kW^{2}s.

5.2 Future work

Future work remains for the development and analysis of a price controlled energy management system at the distribution level. This includes:

- analyzing the economic benefit of the control system
- studying additional use scenarios, including scenarios with no load
- examining the effects of variable latency
- compensating for loss of communication.

Future implementations, possibly at the green energy hub at the FREEDM systems center, could integrate software, hardware and communications into a single system. Additional work to evaluate the practicality of these ideas includes:

- Testing of the energy management on the full IEEE 34 bus test bed
- Utilization of a price profile from a real system
- Examining the interaction and impact of renewable resources in the distribution system.

REFERENCES

[1] United States Department of Energy, "Smart Grid: an Introduction," Office of Electricity Delivery and Energy Reliability, Washington, D.C., 2008.

[2] A. Q. Huang, "The FREEDM System - a Vision for the Future Grid," *IEEE Power and Energy Society General Meeting Proceedings,* pp. 1-4, 2010.

[3] 110th Congress of United States, *Title XIII--Smart Grid,* Washington, DC, December 2007.

[4] Peter Palensky and Dietmar Dietrich, "Demand Side Management: Demand Response, Intelligent Energy Systems, and Smart Loads," *IEEE Transactions on Industrial Informatics,* vol. 7, no. 3, pp. 381-388, August 2011.

[5] Italo Atzeni, Luis G. Ordóñez, Gesualdo Scutari, Daniel P. Palomar and Javier Rodríguez Fonollosa, "Demand-Side Management via Distributed Energy Generation and Storage Optimization," *IEEE Transactions on Smart Grid,* vol. 4, no. 2, June 2013.

[6] F. Maghsoodlou, R. Masiella and T. Ray, "Energy Management Systems," *IEEE Power and Energy Magazine,* vol. 2, no. 5, pp. 49-57, September 2004.

[7] G. Gross and F. D. Galiana, "Short-Term Load Forecasting," *Proceedings of the IEEE,* vol. 75, no. 12, pp. 1558-1573, December 1987.

[8] N. Singh, E. Kliokys, H. Feldmann, R. Kiissel, R. Chrustowski and C. Jaborowicz, "Power System Modelling and Analysis in a Mixed Energy Management and Distribution Management System," *IEEE Transactions on Power Systems,* vol. 13, no. 3, pp. 1143-1149, August 1998.

[9] P. Zhao, S. Suryanarayanan and M. G. Simoes, "An Energy Management System for Building Structures Using a Multi-Agent Decision-Making Control Methodology," *IEEE Transactions on Industry Applications,* vol. 49, no. 1, pp. 322-330, January 2013.

[10] Kathleen Spees and L. B. Lave, "Demand Response and Electricity Market Efficiency," *The Electricity Journal,* vol. 20, no. 3, pp. 69-85, 2007.

[11] "FREEDM Center Goals," NSF FREEDM Systems Center, 2013. [Online]. Available: http://www.freedm.ncsu.edu/. [Accessed 5 June 2013].

[12] A. Q. Huang, M. L. Crow, G. T. Heydt, J. P. Zheng and S. H. Dale, "The Future Renewable Electric Energy Delivery and Management (FREEDM) System: The

Energy Internet," *Proceedings of the IEEE,* vol. 99, no. 1, pp. 133-148, December 2010.

[13] Jesse Boyd and Gerald T. Heydt, "Stability Analysis of an Energy Managed Smart Distribution System," in *IEEE Power and Energy Society General Meeting*, Vancouver, BC, 2013.

[14] D. J. Bolton, "Electricity Demand and Price," *Journal of the Institute of Electrical Engineers,* vol. 82, no. 494, pp. 185-208, February 1938.

[15] G. W. Arnold, "Challenges and Opportunities in Smart Grid: a Position Article," *Proceedings of the IEEE,* vol. 99, no. 6, pp. 922-927, 2011.

[16] J. Wells, "Electricity Markets—Consumers Could Benefit From Demand Programs, But Challenges Remain," Government Accountability Office, Washington, DC, 2004.

[17] C. F. Jack, "Peak Shaving – a Way to Fight Rising Costs," *IEEE Transactions on Industry Applications,* vol. IA 12, no. 5, pp. 486-491, September 1976.

[18] J. Malinowski and K. Kaderly, "Peak Shaving – a Method to Reduce Utility Costs," in *Region 5 Conference: Annual Technical and Leadership Workshop,* April 2004.

[19] Federal Energy Regulatory Commission, "Assessment of Demand Response and Advanced Metering," Staff Report, February 2011.

[20] Federal Energy Regulatory Commission, "A National Assessment of Demand Response Potential," June 2009. [Online]. Available:

http://www.ferc.gov/legal/staff-reports/06-09-demand-response.pdf. [Accessed 4 June 2013].

[21] Peter Palensky and Dietmar Dietrich, "Demand Side Management: Demand Response, Intelligent Energy Systems, and Smart Loads," *IEEE Transactions on Industrial Informatics,* vol. 7, no. 3, pp. 381-388, August 2011.

[22] United States Department of Energy, "Smart Grid: an Introduction," Office of Electricity Delivery and Energy Reliability, Washington DC, 2008.

[23] Antonio J. Conejo, Juan M. Morales and Luis Baringo, "Real-Time Demand Response Mode," *IEEE Transactions on Smart Grid,* vol. 1, no. 3, pp. 236-242, December 2010.

[24] Amit Mohan Saklani, H. S. V. S. Kumar Nunna and Suryanarayana Doolla, "Intelligent Demand Response Approach in Smart Distribution Systems: A Review," in *Annual IEEE India Conference*, December 2012.

[25] Omid Ameri Sianaki, Omar Hussain, Tharam Dillon and Azadeh Rajabian Tabesh, "Intelligent Decision Support System for Including Consumers' Preferences in Residential Energy Consumption in Smart Grid," in *Computational Intelligence, Modelling and Simulation*, September 2010.

[26] Wang and M. de Groot, "Managing End-User Preferences in the Smart Grid," *ACM e-Energy*, pp. 105-114, 2010.

[27] Kamalanath Samarakoon, Janaka Ekanayake and Nick Jenkins, "Reporting Available Demand Response," *IEEE Transactions on Smart Grid*, 2013.

[28] Thillainathan Logenthiran, Dipti Srinivasan, and Tan Zong Shun, "Demand Side Management in Smart Grid Using Heuristic Optimization," *IEEE Transactions on Smart Grid*, vol. 3, no. 3, pp. 1244-1252, September 2012.

[29] Yunfei Wang, Iraj Rahimi Pordanjani and Wilsun Xu, "An Event-Driven Demand Response Scheme for Power System Security Enhancement," *IEEE Transactions on Smart Grid*, vol. 2, no. 1, pp. 23-29, March 2011.

[30] J. Short, D. Infield and L. Freris, "Stabilization of Grid Frequency Through Dynamic Demand Control," *IEEE Transactions on Power Systems*, vol. 22, no. 3, pp. 1284-1293, 2007.

[31] I. Roytelman and V. Ganesan, "Coordinated Local and Centralized Control in Distribution Management Systems," *IEEE Transactions on Power Delivery*, vol. 15, no. 2, pp. 718-724, 2000.

[32] Mohsenian-Rad, V. Wong, J. Jatskevich and R. Schober, "Optimal and Autonomous Incentive-Based Energy Consumption Scheduling Algorithm for Smart Grid," *IEEE Innovative Smart Grid Technologies*, pp. 1-6, January 2010.

[33] Xiang Lu, Wenye Wang and Jianfeng Ma, "An Empirical Study of Communication Infrastructures Towards the Smart Grid: Design, Implementation, and Evaluation," *IEEE Transactions on Smart Grid*, vol. 4, no. 1, pp. 170-183, March 2013.

[34] C. Gellings et al., "Integrating Demand-Side Management into Utility Planning," *IEEE Transactions on Power Systems*, vol. 1, no. 3, pp. 81-87, 1986.

[35] Jose Medina, Nelson Muller and Ilya Roytelman, "Demand Response and Distribution Grid Operations: Opportunities and Challenges," *IEEE Transactions on Smart Grid,* vol. 1, no. 2, pp. 193-198, September 2010.

[36] C. Su and D. Kirschen, "Quantifying the Effect of Demand Response on Electricity Markets," *IEEE Transactions on Power Systems,* vol. 24, no. 3, pp. 1199-1207, 2009.

[37] Dan Yang and Yanni Chen, "Demand Response and Market Performance in Power Economics," in *IEEE Power and Energy Society General Meeting*, July 2009.

[38] F. Rahimi, "Demand Response as a Market Resource under the Smart Grid Paradigm," *IEEE Transactions on Smart Grid,* vol. 1, no. 1, pp. 82-88, June 2010.

[39] Alec Brooks, Ed Lu, Dan Reicher, Charles Spirakis and Bill Weihl, "Demand Dispatch," *IEEE Power and Energy Magazine,* pp. 20-29, June 2010.

[40] H. M. Sayers, "Electricity Supply Tariffs," *Journal of the Institute of Electrical Engineers,* vol. 63, no. 345, pp. 850-856, April 1925.

[41] T. Orfanogianni and G. Gross, "A General Formulation for LMP Evaluation," *IEEE Transactions on Power Systems*, vol. 22, no. 3, pp. 1163-1173, 2007.

[42] M. C. Caramanis, R. E. Bohn and F. C. Schweppe, "Optimal Spot Pricing: Practice and Theory," IEEE Transactions on Power Apparatus and Systems," *IEEE Transactions on Power Apparatus and Systems,* vol. PAS 101, no. 9, pp. 3234-3245, September 1982.

[43] R. E. Bohn, M. C. Caramanis, and F. C. Schweppe, "Optimal Pricing in Electrical Networks over Space and Time," *The RAND Journal of Economics*, vol. 15, no. 3, pp. 360-376, 1984.

[44] S. P. Holland and E. T. Mansur, "The Short-Run Effects of Time-Varying Prices in Competitive Electricity Markets," *Energy Journal,* vol. 27, no. 4, pp. 127-155, 2006.

[45] G. Heydt, Badrul H. Chowdhury, Sr., Maiiesa L. Crow, Daniel A. Haughton, Brian D. Kiefer, Fanjun Meng and Bharadwaj R. Sathyanarayana, "Pricing and Control in the Next Generation Power Distribution System," *IEEE Transactions on Smart Grid.*

[46] C. Gu, J. Wu and F. Li, "Reliability-Based Distribution Network Pricing," *IEEE Transactions on Power Systems*, vol. 1, no. 99, pp. 1-8, 2012.

[47] K. Shaloudegi, N. Madinehi, S. H. Hosseinian and H. A. Abyaneh, "A Novel Policy for Locational Marginal Price Calculation in Distribution Systems Based on Loss Reduction Allocation Using Game Theory," *IEEE Transactions on Power Systems*, vol. 27, no. 2, pp. 811-820, 2012.

[48] Amir Motamedi, Hamidreza Zareipour and William D. Rosehart, "Electricity Price and Demand Forecasting in Smart Grids," *IEEE Transactions on Smart Grid*, vol. 3, no. 2, pp. 664-674, June 2012.

[49] Daniel S. Kirschen, Goran Strbac, Pariya Cumperayot and Dilemar de Paiva Mendes, "Factoring the Elasticity of Demand in Electricity Prices," *IEEE Transactions on Power Systems*, vol. 15, no. 2, May 2000.

[50] M. G. Lijesen, "The Real-Time Price Elasticity of Electricity," *Energy Economics*, vol. 29, pp. 249-258, 2007.

[51] C. Goldman, N. Hopper, R. Bharvirkar, B. Neenan, R. Boisvert, P. Cappers, D. Pratt, and K. Butkins, "Customer Strategies for Responding to Day-Ahead Market Hourly Electricity Pricing," Lawrence Berkeley National Laboratory, Berkeley, CA, 2005.

[52] T. Zachariadis and N. Pashourtidou, "An Empirical Analysis of Electricity Consumption in Cyprus," *Energy Economics*, vol. 29, pp. 183-198, 2007.

[53] T. B. Bjørner and H. H. Jensen, "Interfuel Substitution within Industrial Companies: an Analysis Based on Panel Data at Company Level," *The Energy Journal*, vol. 23, no. 2, pp. 27-50, 2002.

[54] P. G. M. Boonekamp, "Price Elasticities, Policy Measures and Actual Developments in Household Energy Consumption—a Bottom up Analysis for the Netherlands," *Energy Economics*, vol. 29, pp. 133-157, 2007.

[55] Dimitris Bertsimas, David B. Brown and Constantine Caramanis, "Theory and Applications of Robust Optimization," 6 June 2007. [Online]. Available: http://web.mit.edu/dbertsim/www/papers/Robust%20Optimization/Theory%20and%20applications%20of%20robust%20optimization.pdf. [Accessed 26 June 2013].

[56] J. C. Hancock, Introduction to Principles of Communication Theory, McGraw-Hill Inc., 1984.

[57] Jim Eyer and Garth Corey, "Energy Storage for the Electricity Grid: Benefits and Market Potential Assessment Guide," Sandia Report SAND2010-0815, February 2010.

[58] D. Rastler, "Electricity Energy Storage Technology Options," Electric Power Research Institute, Palo Alto, 2010.

[59] Bruce Dunn, Haresh Kamath and Jean-Marie Tarascon, "Electrical Energy Storage for the Grid: a Battery of Choices," *Science,* no. 334, pp. 928-935, November 2011.

[60] Electric Power Research Institute, "Electrical Energy Storage Technology Options," Report 1020676, December 2010.

[61] K.C. Divya and J. Østergaard, "Battery Energy Storage Technology for Power Systems—an Overview," *Electric Power Systems Research,* no. 79, pp. 511-520, 2009.

[62] M. Mortara, "Evaluation of Electric Distribution Losses in Terms of Generating-Station Capacity Investment," *IEEE Transactions on Power Systems,* vol. 64, pp. 1-6, January 1945.

[63] Carlos A. Dortolina and Ramón Nadira, "The Loss That is Unknown is No Loss At All: A Top-Down/Bottom-Up Approach for Estimating Distribution Losses," *IEEE Transactions on Power Systems,* vol. 20, no. 2, pp. 1119-1125, May 2005.

[64] Víctor H. Méndez Quezada, Juan Rivier Abbad and Tomás Gómez San Román, "Assessment of Energy Distribution Losses for Increasing Penetration of Distributed Generation," *IEEE Transactions on Power Systems,* vol. 21, no. 2, pp. 533-540, May 2006.

[65] Xiao Zhang, Feng Gao, Xinjie Lv, Hairong Lv, Qiming Tian, Junhua Ma, Wenjun Yin and Jin Dong, "Line Loss Reduction with Distributed Energy Storage Systems," in *IEEE Power and Energy Society Innovative Smart Grid Technologies Conference,* May 2012.

[66] Hasan Hedayati, S. A. Nabaviniaki, and Adel Akbarimajd, "A Method for Placement of DG Units in Distribution Networks," *IEEE Transactions on Power Delivery,* vol. 23, no. 3, pp. 1620-1628, July 2008.

[67] Hao Qian, Jih-Sheng Lai, Jianhui Zhang and Wensong Yu, "High-Efficiency Bidirectional AC-DC Converter for Energy Storage System," in *IEEE Energy Conversion Congress and Exposition,* September 2010.

[68] M. Durr, A. Cruden, S. Gair and J. McDonald, "Dynamic Model of a Lead Acid Battery for Use in a Domestic Fuel Cell System," *Journal of Power Sources,* vol. 161, pp. 1400-1411, October 2006.

[69] Stephen Boyd and Lieven Vandenberghe, Convex Optimization, Cambridge: Cambridge University Press, 2004.

[70] B. R. Sathyanarayana, "Sensitivity-Based Pricing and Multiobjective Control for Energy Management in Power Distribution Systems," PhD. Thesis, Tempe, AZ, July 2012.

[71] G. T. Heydt, "Multiobjective Optimization: An Educational Opportunity in Power Engineering," *IEEE Transactions on Power Systems*, vol. 24, no. 3, pp. 1631-1632, August 2009.

[72] A. Belegundu and T. Chandrupatla, Optimization Concepts and Applications in Engineering, Englewood Cliffs NJ: Prentice Hall, 1999.

[73] E. Zitzler and L. Thiele, "Multiobjective Evolutionary Algorithms: A Comparative Case Study and the Strength Pareto Approach," *IEEE Transactions on Evolutionary Computation*, vol. 3, no. 4, pp. 257-271, 1999.

[74] D. Van Veldhuizen and G. Lamont, "Multiobjective Evolutionary Algorithms: Analyzing the State of the Art," *IEEE Transactions on Evolutionary Computation*, vol. 8, no. 3, pp. 125-148, 2000.

[75] E. Hughes, "Multiple Single Objective Pareto Sampling," *Proc. Congress on Evolutionary Computation*, vol. 4, pp. 2678-2684, 2003.

[76] I. Das and J. Dennis, "Normal Boundary Intersection: A New Method for Obtaining Pareto Optimal Points in Multicriteria Optimization Problems," *SIAM Journal on Optimization*, vol. 8, no. 3, pp. 631-657, 1998.

[77] "The MOSEK Optimization Toolbox for MATLAB Manual Version 7.0," 2013. [Online]. Available: docs.mosek.com/7.0/toolbox/index.html. [Accessed 13 June 2013].

[78] Claudia D'Ambrosio and Andrea Lodi, "Mixed Integer Nonlinear Programming Tools: an Updated Practical Overview," *Annals of Operations Research*, vol. 204, p. 301–320, 2013.

[79] Stephen P. Boyd and Michael C. Grant, "The CVX Users' Guide," 7 June 2013. [Online]. Available: http://cvxr.com/cvx/doc/CVX.pdf. [Accessed 25 June 2013].

APPENDIX A

MATHCAD FORMULAS, MATLAB CODES AND SIMULINK BLOCK DIAGRAMS

A.1 Use case 1 BIBO stability analysis

Mathcad software was used to formulate the system transfer function *H(z)*. After parameter values were assigned, the poles and zeros of the transfer function were determined and compared for different values of the feedback gain, *B*. The following is the Mathcad code which performed this function. Following the code, Figure A.1 shows the plotted poles and zeros of *H(z)* for B = 0.033 \$/kW^{2}h.

1. Signal formulation

$$\delta(z) := \frac{\delta_0}{1 - z^{-1}} + d(z) + B \cdot z^{-1} \cdot \Delta L(z)$$

$$\Delta\delta(z) := \delta(z) - \frac{\delta_0}{1 - z^{-1}} \rightarrow d(z) + \frac{B \cdot \Delta L(z)}{z}$$

$$E(z) := E_S + \frac{-E_S}{N - 1} \cdot \sum_{n=1}^{N-1} z^{-n}$$

$$\Delta L(z) := \frac{\Delta\delta(z)}{\delta_0} \cdot E(z) \cdot L_0 \rightarrow \frac{L_0 \cdot \left[E_S + \frac{E_S \cdot \left(z^{1-N} - 1\right)}{(N-1) \cdot (z-1)}\right] \cdot \left(d(z) + \frac{B \cdot \Delta L(z)}{z}\right)}{\delta_0}$$

2. Isolation of *ΔL(z)*

$$\frac{L_0 \cdot \left[E_S + \frac{E_S \cdot \left(z^{1-N} - 1\right)}{(N-1) \cdot (z-1)}\right] \cdot \left(d(z) + \frac{B \cdot \Delta L(z)}{z}\right)}{\delta_0} - \Delta L(z) = 0$$

$$\left[\frac{B \cdot L_0 \cdot \left[E_S + \frac{E_S \cdot \left(z^{1-N} - 1\right)}{(N-1) \cdot (z-1)}\right]}{\delta_0 \cdot z} - 1\right] \cdot \Delta L(z) + \frac{L_0 \cdot d(z) \cdot \left[E_S + \frac{E_S \cdot \left(z^{1-N} - 1\right)}{(N-1) \cdot (z-1)}\right]}{\delta_0} = 0$$

$$\Delta L(z) := \frac{-\frac{L_0 \cdot d(z) \cdot \left[E_S + \frac{E_S \cdot \left(z^{1-N} - 1 \right)}{(N-1) \cdot (z-1)} \right]}{\delta_0}}{\left[\frac{B \cdot L_0 \cdot \left[E_S + \frac{E_S \cdot \left(z^{1-N} - 1 \right)}{(N-1) \cdot (z-1)} \right]}{\delta_0 \cdot z} - 1 \right]}$$

3. Derivation of the transfer function *H(z)*

$$H(z) := \frac{-\frac{L_0 \cdot \left[E_S + \frac{E_S \cdot \left(z^{1-N} - 1 \right)}{(N-1) \cdot (z-1)} \right]}{\delta_0}}{\left[\frac{B \cdot L_0 \cdot \left[E_S + \frac{E_S \cdot \left(z^{1-N} - 1 \right)}{(N-1) \cdot (z-1)} \right]}{\delta_0 \cdot z} - 1 \right]}$$

$$H(z) := \frac{E_S \cdot L_0 \cdot \left(z^2 \cdot z^N - z^2 - N \cdot z^2 \cdot z^N + N \cdot z \cdot z^N \right)}{B \cdot E_S \cdot L_0 \cdot \left(z - N \cdot z^N - z \cdot z^N + N \cdot z \cdot z^N \right) + \delta_0 \cdot \left(z^2 \cdot z^N - z \cdot z^N - N \cdot z^2 \cdot z^N + N \cdot z \cdot z^N \right)}$$

4. Finding numerical poles of *H(z)* for system parameter values

$\delta_0 := 0.1$

$N := 24$

$n := 1, 2 .. N - 1$

$L_0 := 10$

$E_S := -0.23$

$$H_d(z) := B \cdot E_S \cdot L_0 \cdot \left(1 - N \cdot z^{N-1} - z^N + N \cdot z^N \right) + \delta_0 \cdot \left(z^{N+1} - z^N - N \cdot z^{N+1} + N \cdot z^N \right)$$

5. *z*-domain pole and zero diagram

The poles and zeros of *H(z)* are plotted in Figure A.1.

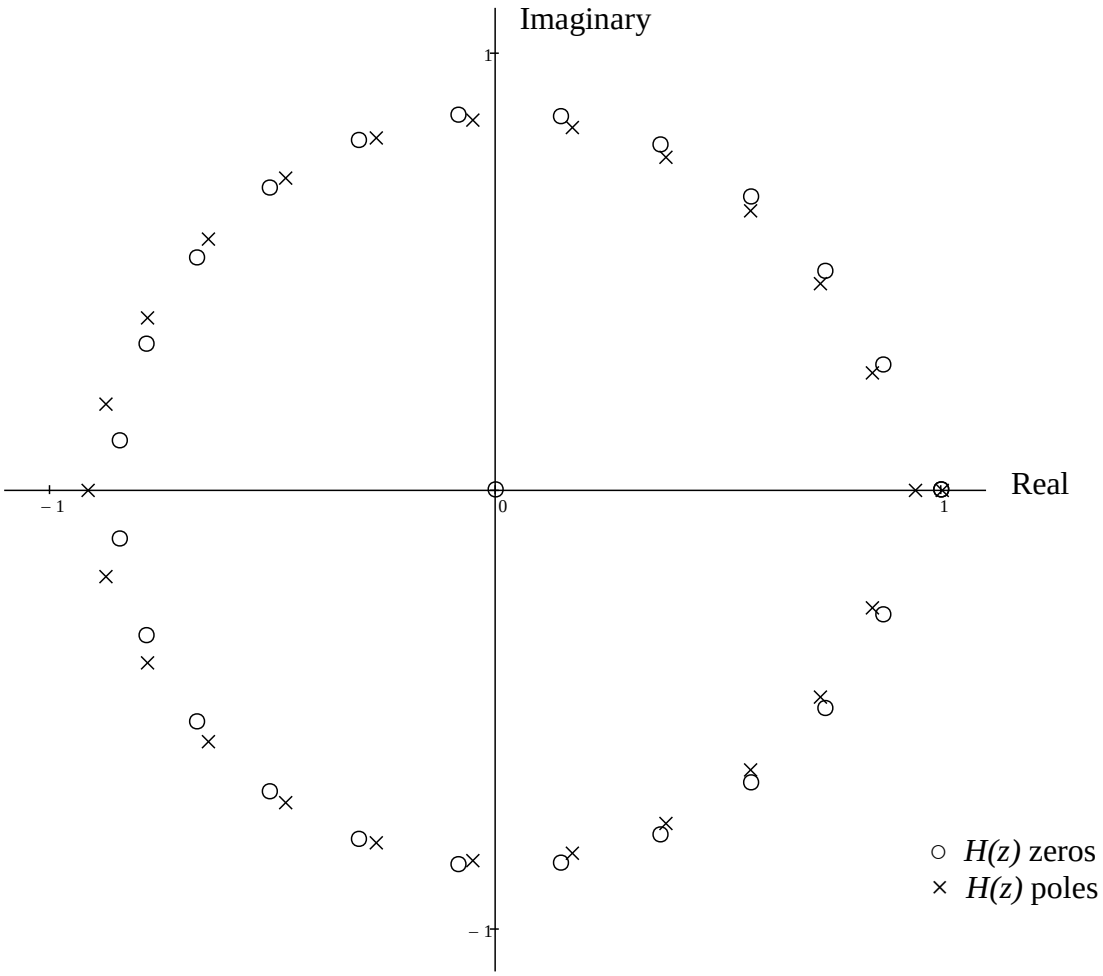

Figure A.1 Use case 1 *z-domain* transfer function pole and zero plot; note the pole and zero at $z = 1$ cancel.

A.2 Use case 1 analytic ISE minimization

The following script was used in Mathcad to derive an analytic formula for ISE and minimize ISE over the feedback gain parameter *B*. This code produced Figure 4.3.

$\$:= ¤$

$j := \sqrt{-1}$

$\delta_0 := 0.1 \cdot \frac{\$}{kW \cdot hr}$

$N := 2^{4}$

$n := 1, 2 .. N - 1$

$L_0 := 10 \cdot kW$

$E_S := -0.2^{3}$

$d_0 := \frac{\delta_0}{10}$

$d(z) := \frac{d_0}{1 - z^{-1}}$

$$H(z, B) := \frac{-\frac{L_0 \cdot \left[E_S + \frac{E_S \cdot \left(z^{1-N} - 1 \right)}{(N - 1) \cdot (z - 1)} \right]}{\delta_0}}{\left[\frac{B \cdot L_0 \cdot \left[E_S + \frac{E_S \cdot \left(z^{1-N} - 1 \right)}{(N - 1) \cdot (z - 1)} \right]}{\delta_0 \cdot z} - 1 \right]}$$

$\Delta L(z, B) := H(z, B) \cdot d(z)$

$\eta(z, B) := \Delta L(z, B)$

$$ISE(B) := \frac{1}{2 \cdot \pi} \cdot \int_0^{2 \cdot \pi} \eta\left(e^{j \cdot \phi}, B\right) \cdot \eta\left(e^{-j \cdot \phi}, B\right) d\phi$$

$B := 0, 0.0001 \frac{\$}{kW^2 hr} .. 0.041 \frac{\$}{kW^2 hr}$

A.3 Use case 1 simulated ISE minimization

The SISO system in use case 1 was created in Simulink. The model diagram is shown in Figure A.2. The B parameter was 'swept' and the simulated ISE values determined for each *B* using the following code. A single B value of 0.033 \$/kW^{2}h was used to show the signal values in the system, shown in Figure A.3.

```
% Calls the B_Parameter_Optimization simulink model with
% different
% values of B and takes the final value of the ISE for
% each B

D = 10/(60*60);          % DLMP forecast (cents/kWs)
B_step = 0.0001;
B_max = 0.041;           % Maximum feedback gain
                         % ($/(kW^2h))
B = (0:B_step:B_max)*(1/60)*(1/60)*100;      % Feedback
                                    % gain (cents/(kWs)^2)
I = zeros(size(B));
i = 1;
for b = B
    simout =
sim('B_Parameter_Optimization','SrcWorkspace','current');
    ISE = simout.get('ISE');
    I(i) = max(ISE)/(60^4)*1000^2; % convert from (kWs)^2
                                   % to (kWh)^2
    i=i+1;
end

plot(B*60*60/100,I,'k','LineWidth',2); % convert B from
                                % cents/(kWs)^2 to $/(kWh)^2
xmin = 0;
xmax = B_max;
ymin = 0.01;
ymax = 0.05;
axis([xmin xmax ymin ymax]);
[value, index] = min(I);
optB = B(index)
ylabel('\it ISE \rm (kW^2s)');
xlabel('\it B \rm parameter $/(kWh)^2');
```

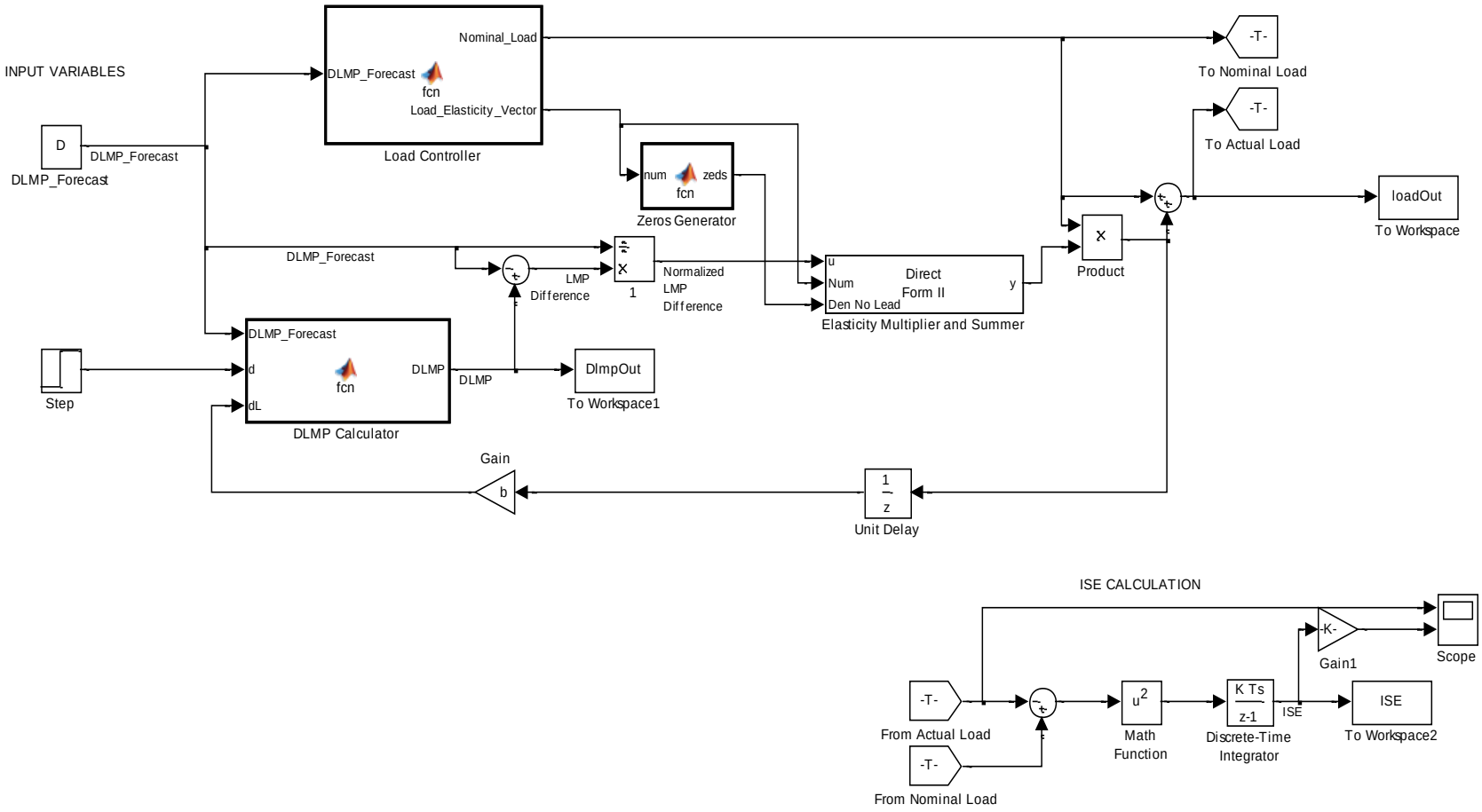

Figure A.2 Use case 1 Simulink model.

```
function DLMP = fcn(DLMP_Forecast, d, dL)
% Calculates the real time DLMP by updating according to
% d and dL

DLMP = DLMP_Forecast + d + dL;
```

```
function [Nominal_Load, Load_Elasticity_Vector]=
fcn(DLMP_Forecast)
% Load control function sets Nominal Load level and Price
% Elasticity values


N = 24;                  %Number of samples per period
Es = -0.23;
Ec = zeros(1,N-1);
Ec = -Es/(N-1)*ones(1,N-1);
%Alternate Ec formula for the linearly decreasing scenario
% x = 2/(N-1);
% dx = 2/(N*(N-1));
% for n = 1:1:N-1
%     Ec(n) = -Es*(x - n*dx);
% end

% Output assignments
Nominal_Load = 10; % kW
Load_Elasticity_Vector = [Es Ec];
```

```
function zeds = fcn(num)
% Generates zeros for the numberator of the transfer
% function coefficients

[row,col] = size(num);
zeds = zeros(row,col-1);
```

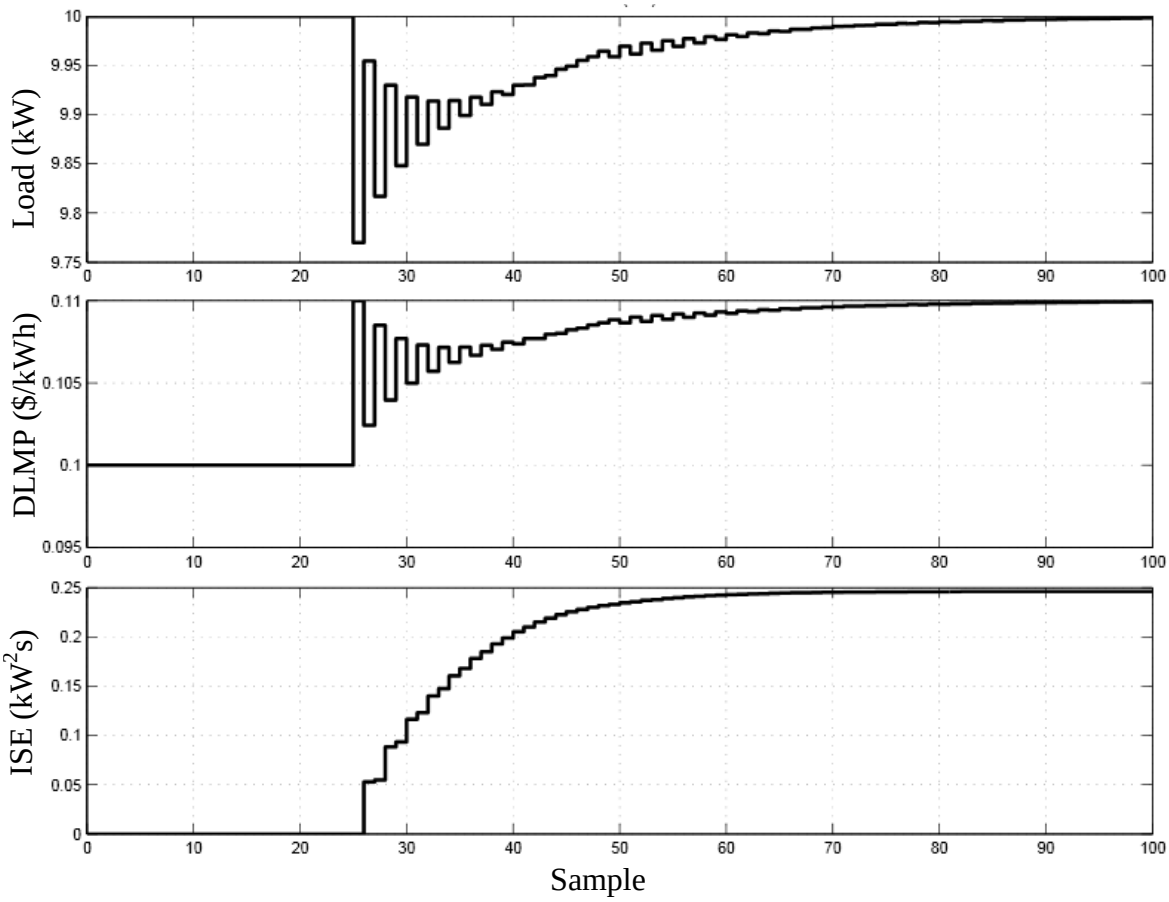

Figure A.3 Use case 1 ISE and real time load level and DLMP price signal for $B = B^*$.

A.4 Use case 2 BIBO stability analysis

The transfer function formula was derived in Mathcad using the below code. The plot in Figure A.4 shows the z-domain poles for three values of the feedback gain *B*. Note the real axis negative pole results in an unstable control system for the highest *B* value.

1. Signal formulas

$$\delta(z,B) := \frac{\delta_0}{1 - z^{-1}} + d(z) + B\cdot z^{-1}\cdot\Delta L(z,B)$$

$$\Delta\delta(z,B) := d(z) + B\cdot z^{-1}\cdot\Delta L(z,B)$$

$$E(z) := E_S + \frac{-E_S}{N-1}\cdot\sum_{n=1}^{N-1} z^{-n}$$

$$\Delta L(z,B) := \frac{\Delta\delta(z,B)}{\delta_0}\cdot E(z)\cdot L_0 \rightarrow -\frac{L_0\cdot\left[E_S + \frac{E_S\cdot\left(z^{1-N}-1\right)}{(N-1)\cdot(z-1)}\right]\cdot\left(\frac{d_0}{\frac{1}{z}-1} - \frac{B\cdot\Delta L(z,B)}{z}\right)}{\delta_0}$$

2. Isolation of *ΔL(z)*

$$\frac{L_0\cdot\left[E_S + \frac{E_S\cdot\left(z^{1-N}-1\right)}{(N-1)\cdot(z-1)}\right]\cdot\left(\frac{B\cdot\Delta L(z,B)}{z} - \frac{0.5}{\frac{1}{z}-1}\right)}{\delta_0} - \Delta L(z,B) = 0$$

$$\left[\frac{B\cdot L_0\cdot\left[E_S + \frac{E_S\cdot\left(z^{1-N}-1\right)}{(N-1)\cdot(z-1)}\right]}{\delta_0\cdot z} - 1\right]\cdot\Delta L(z,B) - \frac{0.5L_0\cdot\left[E_S + \frac{E_S\cdot\left(z^{1-N}-1\right)}{(N-1)\cdot(z-1)}\right]}{\delta_0\cdot\left(\frac{1}{z}-1\right)} = 0$$

$$\Delta L(z,B) := \frac{\frac{0.5\cdot L_0\cdot\left[E_S + \frac{E_S\cdot\left(z^{1-N}-1\right)}{(N-1)\cdot(z-1)}\right]}{\delta_0\cdot\left(\frac{1}{z}-1\right)}}{\left[\frac{B\cdot L_0\cdot\left[E_S + \frac{E_S\cdot\left(z^{1-N}-1\right)}{(N-1)\cdot(z-1)}\right]}{\delta_0\cdot z} - 1\right]}$$

3. Derivation of the transfer function *H(z)*

$$H(z,B) := \frac{-\dfrac{L_0\cdot\left[E_S - \dfrac{E_S\cdot\left(2\cdot z^{1-N} - 2\cdot z - 2\cdot N + 2\cdot N\cdot z\right)}{N\cdot(N-1)\cdot(z-1)^2}\right]}{\delta_0}}{\left[\dfrac{B\cdot L_0\cdot\left[E_S - \dfrac{E_S\cdot\left(2\cdot z^{1-N} - 2\cdot z - 2\cdot N + 2\cdot N\cdot z\right)}{N\cdot(N-1)\cdot(z-1)^2}\right]}{\delta_0\cdot z} - 1\right]}$$

4. Plotting *z*-domain poles of *H(z)* for system parameter values

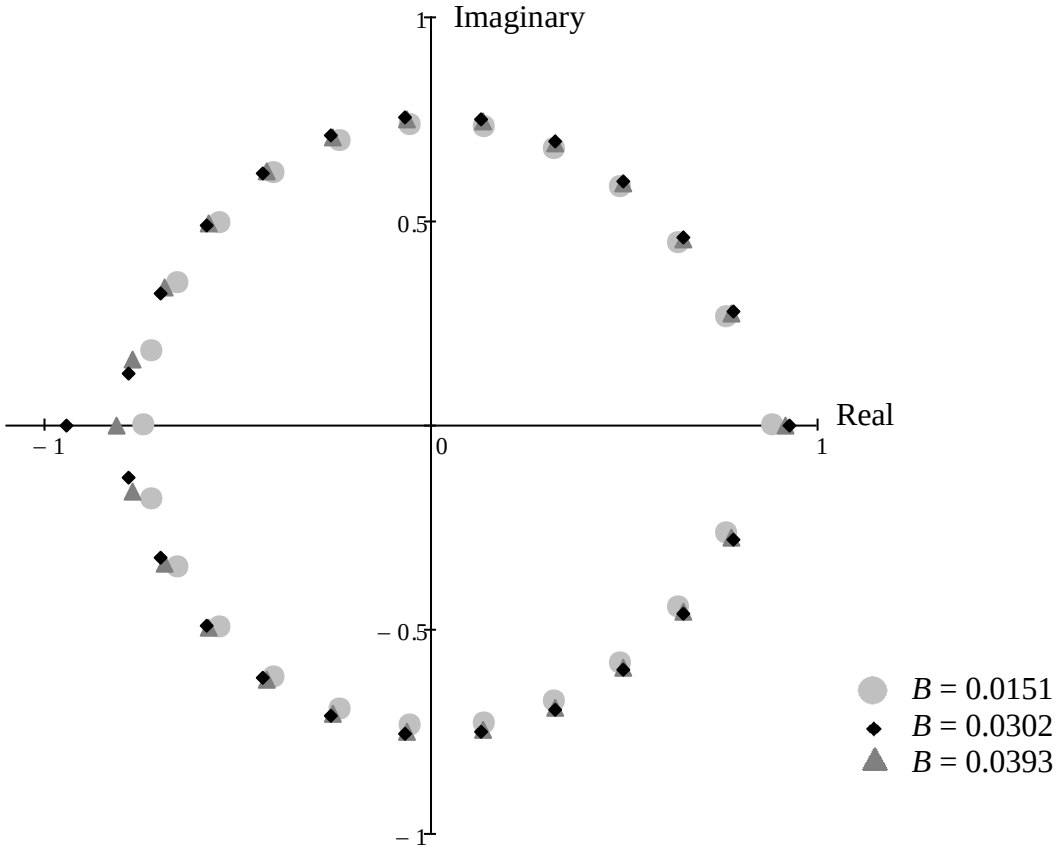

Figure A.4 SISO system stransfer function z-domain poles for case l scenario 2.

A.5 Use case 2 analytic ISE minimization

The following script was used in Mathcad to produce Figure 4.5

$$d(z) := \frac{d_0}{1 - z^{-1}}$$

$$H(z,B) := \frac{-\dfrac{L_0 \cdot \left[E_S - \dfrac{E_S \cdot \left(2 \cdot z^{1-N} - 2 \cdot z - 2 \cdot N + 2 \cdot N \cdot z\right)}{N \cdot (N-1) \cdot (z-1)^2}\right]}{\delta_0}}{\left[\dfrac{B \cdot L_0 \cdot \left[E_S - \dfrac{E_S \cdot \left(2 \cdot z^{1-N} - 2 \cdot z - 2 \cdot N + 2 \cdot N \cdot z\right)}{N \cdot (N-1) \cdot (z-1)^2}\right]}{\delta_0 \cdot z} - 1\right]}$$

$$\Delta L(z,B) := H(z,B) \cdot d(z)$$

$$\eta(z,B) := \Delta L(z,B)$$

$$ISE(B) := \frac{1}{2 \cdot \pi} \cdot \int_0^{2 \cdot \pi} \eta\left(e^{j \cdot \phi}, B\right) \cdot \eta\left(e^{-j \cdot \phi}, B\right) d\phi$$

$$B := 0, 0.0001 \frac{\$}{kW^2 hr} .. 0.041 \frac{\$}{kW^2 hr}$$

A.6 Use case 3 simulated ISE minimization

The Simulink functional blocks were recoded with the following code for use case 3. This code produced the data in Figure 4.6.

```
function [norm_dL, norm_dL_next] = fcn(E, norm_dLMP,
norm_dL_delayed)
% This function takes as inputs the price elasticity
% values, delta_LMP vector,
% delta_Load_prior vector and determines the change in
% load. It also passes
% on the cross-price elasticity load change for the next
% samples.

[rows, cols] = size(E);
% Present change in load
norm_dL = norm_dLMP.*E(:,1) + norm_dL_delayed(:,1);
% First contribution to the load change is the self-price
% elasticity, the second is the cross-price elasticity
% Future changes in load
norm_dL_delayed = circshift(norm_dL_delayed,[0,-1]);
% Shift the previous load changes to the next position in
% the matrix
% The norm_dL_delayed matrix is arranged in the order
% [z^-1 z^-2 z^-3...
% z^-1 z^-2...]
norm_dL_delayed(:,cols-1) = zeros(rows,1);   % replace the
% last row with zeros; this row will be added to by the
% present price change
norm_dL_next = zeros(rows,cols-1);
for n = 1:1:rows
    norm_dL_next(n,:) = norm_dL_delayed(n,:) +
E(n,2:cols).*norm_dLMP(n); % present change in price
% contributes to the future load changes according to
% cross-price elasticity values
end
```

```
% Calls the B_Parameter_Optimization simulink model with
% different
% values of B and takes the final value of the ISE for
% each B

D = [10/(60*60);0];          % DLMP forecast (cents/kWs)
B_step = 0.0005;
B_max = 0.040;           % Maximum feedback gain
                         % ($/(kW^2h))
B_diag = (0:B_step:B_max)*(1/60)*(1/60)*100;       % Feed
                                % back gain (cents/(kWs)^2)
B_off_diag = (-B_max:B_step:B_max)*(1/60)*(1/60)*100;
% Feedback gain (cents/(kWs)^2)
I = zeros(B_max/B_step + 1, B_max/B_step + 1);
i = 1;
for b_diag = B_diag
    j = 1;
    for b_off_diag = B_off_diag
        B_Matrix = [b_diag b_off_diag; b_off_diag b_diag];
        simout =
sim('MIMO_ISE_Model','SrcWorkspace','current');
        ISE = simout.get('ISE');
        I(i,j) = max(ISE)/(60^4)*1000^2; % convert from
                                         % (kWs)^2 to (kWh)^2
        j = j+1;
    end
    i=i+1;
end

surf(B_off_diag*60*60/100, B_diag*60*60/100,I); % convert
B from cents/(kWs)^2 to $/(kWh)^2
xmin = -B_max;
xmax = B_max;
ymin = 0;
ymax = B_max;
zmin = 0.015;
zmax = 0.05;
axis([xmin xmax ymin ymax zmin zmax]);
zlabel('\it ISE \rm (Wh)^2');
xlabel('\it B_1_2 \rm parameter $/(kWh)^2');
ylabel('\it B_1_1 \rm parameter $/(kWh)^2');
caxis([zmin, zmax]);
colormap((transpose(zmax - linspace(zmin, zmax))/(zmax-
zmin))*[1 1 1]);
shading interp;
```

A.7 Use case 4 battery flow optimization

The following code was used in Mathcad to find the least squares fit to a low loss power converter loss characteristic curve from [67]. The function *f* represents the percentage of real power loss as a function of power generated. Therefore, *f* times *x* would represent loss (in kW). This is matched to an efficiency curve to find the coefficients a, b and c. This code was used to produce the graph in Figure A.5.

$$f(a,b,c,x) := a\cdot x + b + \frac{c}{x}$$

Initial Guesses

$a := -0.5$

$b := 0.5$

$c := 0$

Solve Block

Given

$f(a,b,c,0.3) = 0.036$

$f(a,b,c,0.6) = 0.028$

$f(a,b,c,1.2) = 0.022$

$$\begin{pmatrix} A \\ B \\ C \end{pmatrix} := \text{Find}(a,b,c) = \begin{pmatrix} -0.004444444 \\ 0.024 \\ 0.004 \end{pmatrix}$$

Having solved for the coefficients, the function p_{loss} is made to calculate power loss in kW for each power production value (p).

$$p_{loss}(p) := f\left(\frac{A}{kW}, B, C\cdot kW, p\right)\cdot p$$

$p := 0kW, 0.01kW .. 1.5kW$

$$\varepsilon(p) := 1 - \frac{p_{loss}(p)}{p}$$

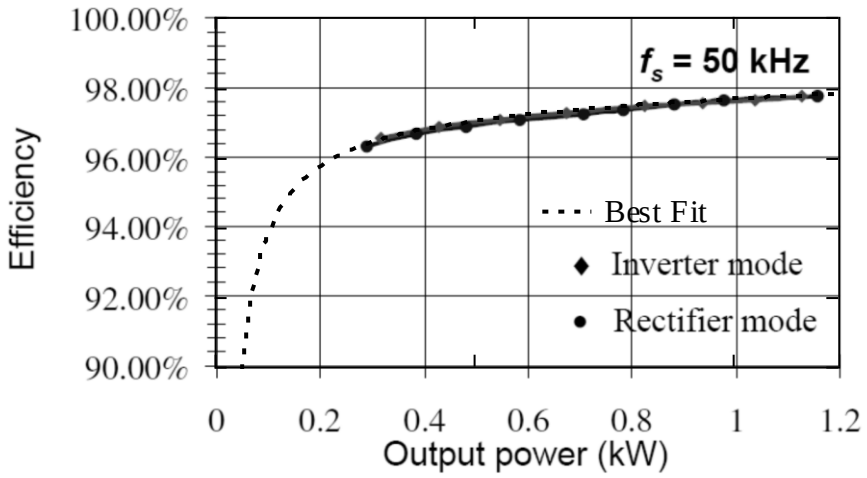

Figure A.5 Comparison between the best-fit approximation and the high-efficiency power converter design from [67].

The battery flow optimization program was developed in Matlab by a calling function and a called function, with code shown below. The initial battery flow solution yielded the results shown in Figure A.6. After the weight w_2 was adjusted to level the battery power flow, the results obtained were those of Figure A.7.

```
%-------------------------------------------------------------
% Distributed energy storage optimization program
%-------------------------------------------------------------
cvx_solver mosek

% Samples
N = 24;                  % number of samples per day

% Multi-objective optimization weights
w2 = 0.1044;
[BSOC_max] = DESD_Opt_Norm(w2, N);
i = 1;

while (BSOC_max > 4.9999) && (i < 10)   % w2 assures
                                        % capacity > BSOC
    w2 = w2 + 0.00001;
    [BSOC_max] = DESD_Opt_Norm(w2, N);
    i = i + 1;
end
```

```
function [ BSOC_max] = DESD_Opt_Norm(w2, N)
% DESD_Opt_Norm performs multi-objective optimization for
% weights w2 and w1 = 1

n = transpose(1:N);      % n represents sample
T = 24/N;                % sample time period (hours)

% Electric energy cost creation
c = 1 - 0.5 * cos(2 * pi * n / N);  % generic load profile
c = c * 20 / 3 / 100;               % energy price $/kWh

% Squared loss formulas
ALPHA = zeros(N);        % power loss coefficient matrix
                         % in kW^-1; note this is used for
                         % the cvx program which requires
                         % the objective function in the
                         % form x'*P*x
CHI = zeros(N);   % power loss coefficient matrix in kW^-1
alpha = 0;      % g^2 multiplier
chi = 0;      % s^2 multiplier
beta = 0;      % g multiplier (%)
psi = 0;      % s multiplier (%)

% Battery characterization
Rbatt = 0.06;      % 60 milliohms
Vbatt = 72;         % 72V lead acid battery
loss_battery = Rbatt / Vbatt^2 * 1000;  % multiplier for
                % s^2 and g^2 to model battery loss (1/kW)
alpha = loss_battery + alpha;      % g^2 multiplier
chi = loss_battery + chi;      % s^2 multiplier
Bmax = 5;               % kWh battery capacity
Bmin = 0;                % minimum battery charge kWh
B0 = (Bmax + Bmin) / 2;       % Initial battery charge kWh

% Power electronic converter characterization
% power converter loss (in percentage)
pConv2 = -0.004444; % square term (kW^-1)
pConv1 = 0.024; % x coefficient (%)
pConv0 = 0.004;  % constant (kW)
beta = beta + pConv1;
psi = psi + pConv1;
alpha = alpha + pConv2;
chi = chi + pConv2;
gamma = pConv0;      % kW loss constant for g
omega = pConv0;      % kW loss constant for s
Pmax = 1.3;      % kW maximum for power converter
```

```
Pmin = 0;      % kW minimum for power converter

% Squared loss formulas
ALPHA = alpha*diag(c)*T;    % power loss coefficient matrix
                            % in $/(kW^2); note this is
                            % used for the cvx program
                            % which requires the objective
                            % function in the form x'*P*x
CHI = chi*diag(c)*T;        % power loss coefficient matrix
                            % in $/(kW^2)

% Optimization using cvx software
sz = size(c);
L = tril(ones(N));     % lower triangle of ones for BSOC
                       % constraint
I = eye(N);

psi = psi*c'*T;
beta = beta*c'*T;
w2 = w2*T;

% BINARY VARIABLE optimization represents the on and off
% states of the battery
cvx_begin
    variables s(sz) g(sz) B0;      % Optimization variables
     % g - power out, s - power in in kW for each sample
     % u,v - commit to charge or discharge
    variable u(sz) binary;
    variable v(sz) binary;
    minimize(s'*CHI*s + psi*s + c'*T*s + c'*T*u*omega -
c'*T*g + g'*ALPHA*g + beta*g + c'*T*v*gamma + w2*norm(s +
g)^2);
    subject to
        sum(s-g) * T == 0;  % Balance of charge constraint
        Bmin - B0 <= L * s * T - L * g * T <= Bmax - B0;
% BSOC constraint, shadow price y ($/kWh) is the value of
% the next kWh of battery capacity
        Pmin * u <= s <= Pmax * u;  % When u = 0, s = 0
        Pmin * v <= g <= Pmax * v;  % When v = 0, g = 0
        u + v <= 1;     % Either v or u may be 1, not both
cvx_end
```

```
% DUAL VARIABLE optimization allows the calculation of
% shadow prices
cvx_begin
    variables s(sz) g(sz) B0;
    dual variables w x y z
    minimize(s'*CHI*s + psi*s + c'*T*s + c'*T*u*omega -
c'*T*g + g'*ALPHA*g + beta*g + c'*T*v*gamma + w2*norm(s +
g)^2);
    subject to
        x: sum(s-g) * T == 0;      % Dual interpretation:
            % value of each kWh of charged energy ($/kWh)
        y: Bmin - B0 <= L * s * T - L * g * T <= Bmax -...
B0; %y interpretation: value of extra battery capacity
    %($/kWh)
        z: Pmin * u <= s <= Pmax * u;  % z interpretation:
                    % value of next unit of storage flow
        w: Pmin * v <= g <= Pmax * v;  % w interpretation:
                    % value of next unit of generation flow
cvx_end

charge_price = x;
discharge_price = sum(y)+x;

% Display results
fig = 1;
h = n*24/N;
figure(fig);
fig = fig+1;

subplot(3,1,1);
plot(h,(s - g), 'LineWidth', 2);
% Power flow into and out of battery as determined by kWh
% per sample / time per sample in hours
ylabel('Battery demand (kW)');
axis tight;
subplot(3,1,2);
plot(h,c*100,h,charge_price*100*ones(size(h)),h,...
   discharge_price*100*ones(size(h)), 'LineWidth', 2);
% TLMP in cents / kWh
ylabel('Price (c/kWh)');
axis tight;

subplot(3,1,3);
BSOC = B0 * ones(sz) + L * (s - g) * T;
plot(h,BSOC, 'LineWidth', 2);  % BSOC
xlabel('Hour (h)');
```

```
ylabel('BSOC (kWh)');
axis tight;

% Plot the losses and the costs of the losses to justify
% the total profit
figure(fig);
fig = fig + 1;
loss_pConv = (pConv2*(s+g).^2 + pConv1*(s+g) + omega*u
+gamma*v);    % 3 terms
loss_battery = (loss_battery*(s+g).^2);  % 1 term
plot(n, loss_pConv*1000, n, loss_battery*1000, 'Lin-
eWidth', 2)
legend('Power Converter', 'Battery')
ylabel('Loss (W)')

BSOC_max = max(BSOC);
delta_q = 1;% percent change in demand (from full to zero)
delta_p = (max(c) - discharge_price) / max(c);
       % percent change in price (from highest to lowest)
mu = delta_q / delta_p
generation = max(g)
end
```

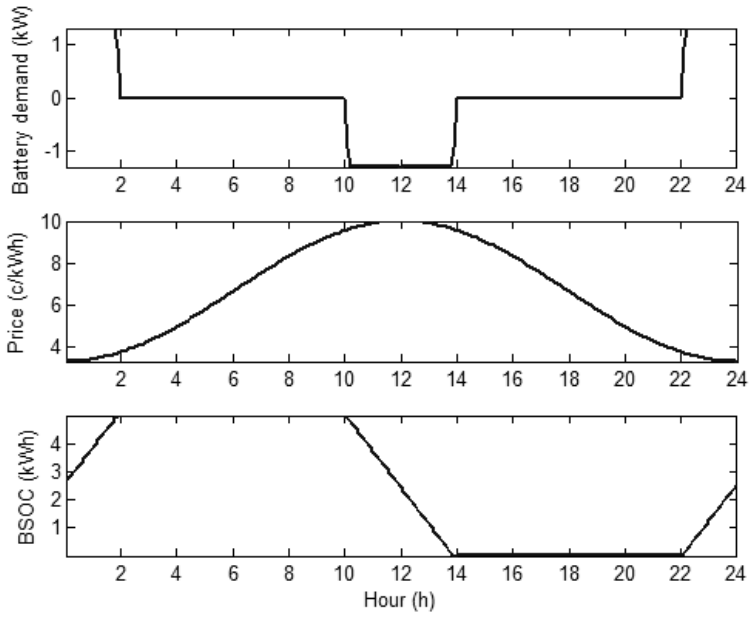

Figure A.6 Solution to the battery flow optimization problem with $w_2 = 0$; note the large jumps in power levels.

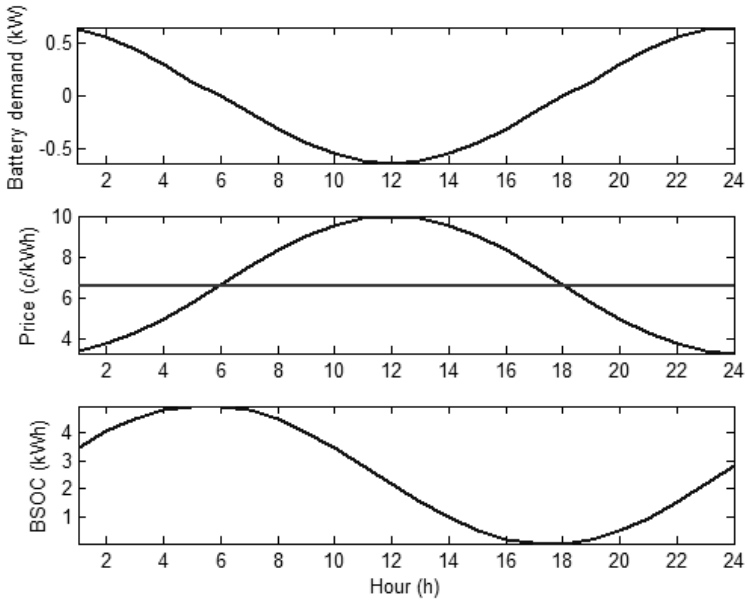

Figure A.7 Battery flow and state of charge for $w_2 = 0.1044$ \$/kWh.

A.8 Use case 4 simulated ISE minimization

The battery was added as a second load to the Simulink system as shown in Figure A.8.

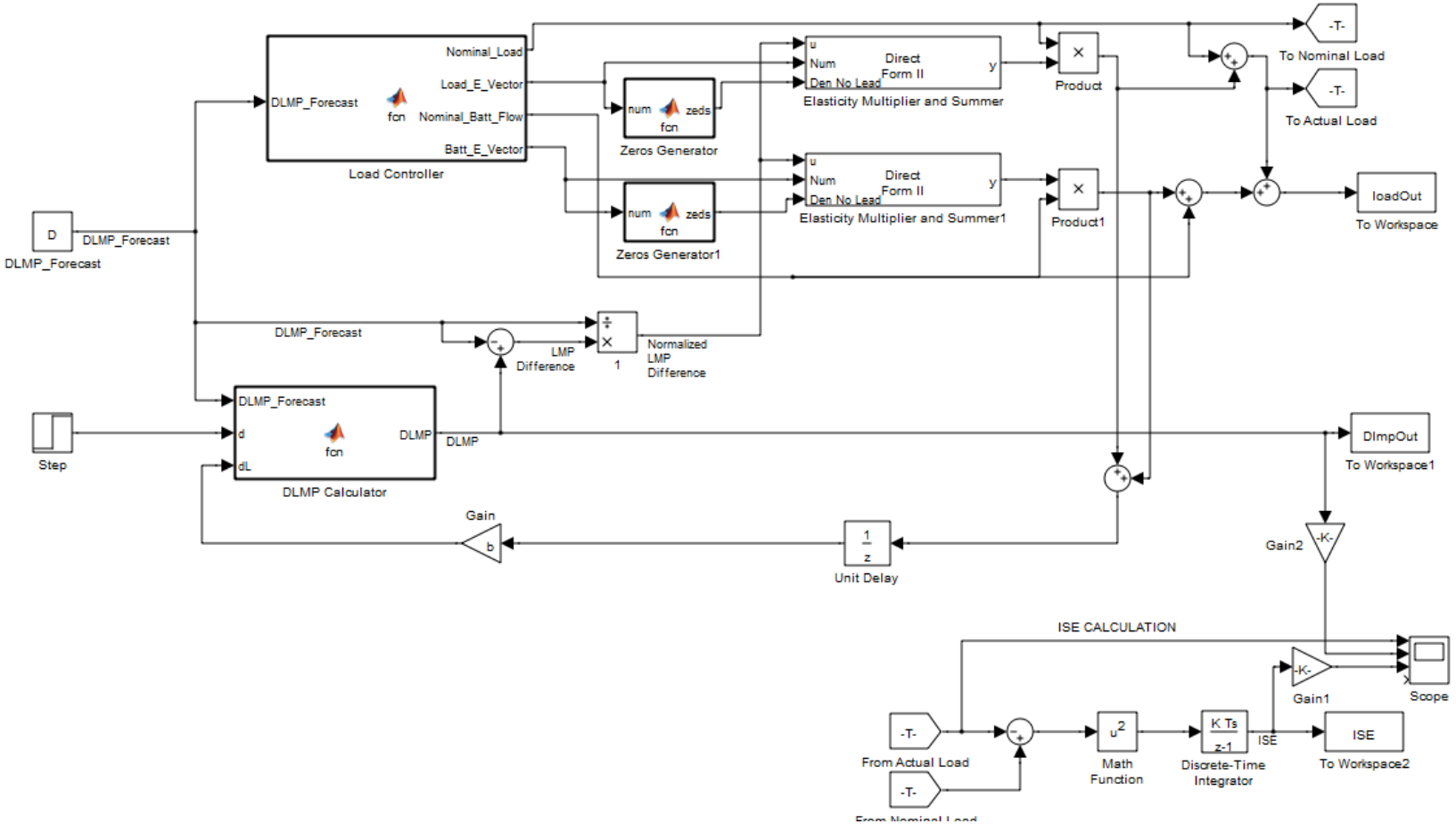

Figure A.8 Use case 4 Simulink model; note two distinct output signals and elasticity multiplier functions.

```
function [Nominal_Load, Load_E_Vector, Nominal_Batt_Flow,
Batt_E_Vector]= fcn(DLMP_Forecast)
% Load control function sets Nominal Load level and Price
% Elasticity values


N = 24;                    %Number of samples per period

Es = -0.23;             %self-elasticity of controllable load
Ec = zeros(1,N-1);
Ec = -Es/(N-1)*ones(1,N-1);       %cross-elasticity of con
                                  % trollable load

Es_b = 2.97;                      %self-elasticity of
                                  % battery demand
Ec_b = -Es_b/(N-1)*ones(1,N-1);   %cross-elasticity of
                                  % battery demand

% Output assignments
Nominal_Load = 10; % kW
Load_E_Vector = [Es Ec];

Nominal_Batt_Flow = -0.67; % kW
Batt_E_Vector = [Es_b Ec_b];
```

A.9 Use case 5 simulated ISE minimization

The following code was used to call different load levels at a normal distribution for the robust minimization of ISE. Note that for an unbounded output the ISE is infinite but for the 100 sample time limit in the simulation, the ISE of an unbounded signal is finite. This code produced Figure 4.8 and Figure 4.9.

```
% Calls the B_Parameter_Optimization simulink model with
% different
% values of B and takes the final value of the ISE for
% each B

D = 10/(60*60);          % DLMP forecast (cents/kWs)
B_step = 0.0001;
B_max = 0.03;           % Maximum feedback gain ($/(kW^2h))
Loads = 5:15;          % range of load levels
B = (0:B_step:B_max)*(1/60)*(1/60)*100;      % Feedback
                                        % gain cents/(kWs)^2)
I = zeros(size(Loads));
ISE_total = zeros(size(B));

prob_L = pdf('Normal',-7:7,0,1);

j = 1;
for b = B
    i = 1;
    for L = Loads
        simout =
sim('B_Parameter_Optimization','SrcWorkspace','current');
        ISE = simout.get('ISE');
        I(i) = max(ISE)/(60^4)*1000^2 * prob_L(i);
                          % convert from (kWs)^2 to (kWh)^2
        i=i+1;
    end
    ISE_total(j) = sum(I);
    j = j + 1;
end

plot(B*60*60/100,ISE_total,'k','LineWidth',2);
                % convert B from cents/(kWs)^2 to $/(kWh)^2
xmin = 0;
xmax = B_max;
ymin = 0;
ymax = min(ISE_total)*10;
axis([xmin xmax ymin ymax]);
[value, index] = min(ISE_total);
optB = B(index)
ylabel('\it ISE \rm (Wh)^2');
xlabel('\it B \rm parameter $/(kWh)^2');
```